Scalar Neutrinos at the LHC

Durmuş A. Demir[a], Mariana Frank[b], Levent Selbuz[a,c], and Ismail Turan[d]

[a]*Department of Physics, İzmir Institute of Technology, IZTECH, TR35430 İzmir, Turkey,*

[b]*Department of Physics, Concordia University,*

7141 Sherbrooke St. West, Montreal, Quebec, Canada H4B 1R6,

[c]*Department of Engineering Physics,*

Ankara University, TR06100 Ankara, Turkey, and

[d]*Ottawa-Carleton Institute of Physics, Carleton University,*

1125 Colonel By Drive Ottawa, Ontario, Canada, K1S 5B6.

Abstract

We study a softly-broken supersymmetric model whose gauge symmetry is that of the standard model (SM) gauge group times an extra Abelian symmetry $U(1)'$. We call this gauge-extended model $U(1)'$ model, and we study a $U(1)'$ model with a secluded sector such that neutrinos acquire Dirac masses via higher-dimensional terms allowed by the $U(1)'$ invariance. In this model the μ term of the minimal supersymmetric model (MSSM) is dynamically induced by the vacuum expectation value of a singlet scalar. In addition, the model contains exotic particles necessary for anomaly cancellation, and extra singlet bosons for achieving correct Z'/Z mass hierarchy. The neutrinos are charged under $U(1)'$, and thus, their production and decay channels differ from those in the MSSM in strength and topology. We implement the model into standard packages and perform a detailed analysis of sneutrino production and decay at the Large Hadron Collider, for various mass scenarios, concentrating on three types of signals: *(1)* $0\ell + \text{MET}$, *(2)* $2\ell + \text{MET}$, and *(3)* $4\ell + \text{MET}$. We compare the results with those of the MSSM whenever possible, and analyze the SM background for each signal. The sneutrino production and decays provide clear signatures enabling distinction of the $U(1)'$ model from the MSSM at the LHC.

CONTENTS

I. INTRODUCTION AND MOTIVATION

The MSSM is arguably the most popular 'new physics' scenario referring to a perturbative completion of the SM beyond Fermi energies. Motivated by the resolution of such long standing problems of the SM as the gauge hierarchy problem, the existence of dark matter and the added attraction of gauge unification, nevertheless, it still has some outstanding problems. One of these is the so-called μ problem [1]. Supersymmetric models which extend the MSSM via an extra gauge group generally intend to solve μ problem and incorporate an extra singlet field, whose coupling to the Higgs fields and VEV generate dynamically the μ

term. These models extend the $SU(2)_L \otimes U(1)_Y$ MSSM electroweak symmetry by an extra $U(1)$ gauge symmetry. Such an extension is minimal, and it is well motivated in superstring theories [2], grand unified theories [3] and in dynamical electroweak breaking theories [4]. The simplest versions contain a singlet field and an extra neutral gauge boson. Other versions also allow right-handed neutrinos into the spectrum. In a non-minimal version of the $U(1)$ extended MSSM, which includes several singlet (S) fields, the tension between the electroweak scale and developing a large enough Z' mass is resolved. We call this version of the model *secluded sector $U(1)'$*, a shorthand notation for $SU(3)_c \otimes SU(2)_L \otimes U(1)_Y \otimes U(1)'$, the gauge symmetry underlying the model, and describe it in the next section. In the MSSM, as in the SM, neutrinos are massless. The fact that neutrino oscillation imply non-vanishing neutrino masses is a strong motivation to consider an extended form of the MSSM. Small neutrino masses consistent with neutrino oscillation phenomenology are usually explained by the see-saw mechanism [5]. In the see-saw mechanism, large Majorana masses for right-handed neutrinos induce small Majorana masses for left-handed neutrinos. In the scalar sector, right-handed sneutrinos mix with the left handed sneutrinos and give potentially new signals for extended symmetry. The choice of $U(1)$ symmetry would determine the magnitude and type of neutrino masses. In this paper, we consider a $U(1)'$ extended form of the MSSM that contains Dirac-type neutrino masses.

Direct or indirect detection of the superpartners of the Standard Model particles, the definitive signal for supersymmetry, is one of the major aims of the LHC experiments. Except for the LSP in the $R-$parity conserving supersymmetry, the superpartners are expected to decay instantaneously into SM particles, plus the LSP, detected as missing energy. The common methodology for detection is to analyze the production and cascade decays of the supersymmetric particles. As the right sneutrinos, which can mix with the left sneutrinos are a feature of the $U(1)'$ model that distinguishes it from MSSM, studying sneutrino signals would be an important test for this model.

Systematic analyses of sneutrino decays in the MSSM have been performed in [6]. The aim of this article is to perform a comparative study of LHC signals of sneutrino production and decays in the MSSM and in a supersymmetric model with a secluded $U(1)'$ breaking sector [7] via their decay chain topologies. Differences between MSSM and the *secluded sector $U(1)'$* model likely reveal themselves via decay modes of the sneutrino. We analyze the signals, and, for completeness, we also include possible Standard Model backgrounds.

In most variants of the MSSM consistent with relic density calculations, the LSP is the lightest neutralino, typically a mixed state of bino (fermionic partner of the $U(1)_Y$ gauge boson) and the higgsino. In a previous work [8], we showed that a minimal $U(1)'$ model (one extra singlet boson) could be consistent with the excess positron observed in satellite experiments, choosing on of the right-handed sneutrinos as the LSP. However, for the purpose of this work (dependent on parameter space chosen to compare our results with those of MSSM), the *secluded sector* $U(1)'$ lightest neutralino appears consistently to be the lightest supersymmetric particle (LSP) and therefore is a potentially viable dark matter (DM) candidate, although its composition is likely to differ from the lightest neutralino in MSSM.

Here we perform a thorough analysis of sneutrino production and decay in the *secluded sector* $U(1)'$ model. In order to compare with previous signals, we establish a set of three mSUGRA-inspired benchmarks for our model. Similar to the mSUGRA benchmark points analyzed in MSSM (LM1, LM2, LM6) [9–11], we analyze the corresponding scenarios in *secluded sector* $U(1)'$ model (LM1$'$, LM2$'$, LM6$'$). Here LM stands for Low Mass, a choice likely to yield visible signals at the LHC.

Our paper is organized as follows. We briefly introduce the model in Section II, then define the parameters and physical masses of supersymmetric particles in the *secluded sector* $U(1)'$ model in Section III. For each benchmark point, we insure that DM candidate of the $U(1)'$ model yields relic densities consistent with the WMAP range of cold dark matter density [12]. We then perform a comparative analysis of the production, decays and detectability of sneutrinos within these benchmark supersymmetric scenarios. During this analysis we focus on the multilepton plus missing energy signatures of the supersymmetric scenarios. We present the results of our simulation analysis for the LHC. In Section IV we conclude the work. We leave the extensive details of the model for the Appendices.

II.   THE $U(1)'$ MODEL

The MSSM suffers from a naturalness problem due to the presence of μ parameter, responsible for giving masses to the Higgs bosons and Higgsino in the superpotential. From a purely theoretical point of view, the value of this parameter is expected to be either of the order of the GUT, Planck scale or zero. For phenomenological aspects, however, it must be

of the order of the scale of electroweak symmetry breaking (EWSB) and it has to be non-zero to agree with the experimental data. Seen from the low energy point of view, adding an extra $U(1)$ is needed in order to solve the μ problem [1] of the MSSM. Basically the problem is remedied by extending the matter and gauge structure of the MSSM, *e.g.* within unified and/or string models by introducing an additional singlet filed S, whose VEV generates the μ term dynamically. Theories with an extra $U(1)'$ broken at the electroweak- to- TeV scale by SM singlets are known to be able to generate an appropriately sized μ parameter (see *e.g.* [1]).

The other success of the $U(1)'$ symmetry is being able to generate pertinent neutrino masses by introducing right-handed neutrinos into the superpotential. The right-handed neutrino sector and the μ parameter can be correlated for both Majorana [13] and Dirac masses [14]. We assume here that lepton number is an accidental symmetry that is conserved at the perturbative level. Hence, the neutrinos are Dirac fermions, requiring Yukawa couplings of $\mathcal{O}\left(10^{-13}\right)$. These couplings are technically natural, but an explanation for such a strong suppression is clearly desirable. One way this can occur is if the $U(1)'$ invariance suppresses leading order contributions to Dirac neutrino masses and allows higher-dimensional operators [14].

In this work, we extend the MSSM in the following ways. First, the gauge structure of the MSSM, $SU(3)_C \otimes SU(2)_L \otimes U(1)_Y$, is enriched to include an extra Abelian group factor $U(1)'$. Second, we promote the μ parameter into dynamical field, S, which is charged under the $U(1)'$. Third, exotics with Yukawa couplings to S are included to make the theory anomaly-free. Fourth, Z'/Z mass hierarchy in the model is ensured by three additional $SU(2)$ singlet fields which are coming from secluded sector of the model. The model also includes a term that provides suppressed Dirac neutrino masses in accordance with observations. We present the main relevant points in this section, leaving the details for the appendices.

In the minimal version of the model which contains only one singlet S, there is some tension between the electroweak scale and the need to generate a large enough M_Z'. These two problems can be decoupled without fine tuning when several additional fields are incorporated into the model. An example of this kind of non-minimal model is *secluded sector model*. The secluded sector model involves an ordinary sector of symmetry breaking fields, which includes two Higgs doublets, and an $SU(2)_L$ singlet S. After acquiring a VEV, S generates an effective μ parameter $\mu = h_s \langle S \rangle$. The secluded sector of the model includes

Field	$\widehat{Q}$	$\widehat{U}$	$\widehat{D}$	$\widehat{L}$	$\widehat{N}$	$\widehat{E}$	$\widehat{H}_u$	$\widehat{H}_d$	$\widehat{S}$	$\widehat{S}_1$	$\widehat{S}_2$	$\widehat{S}_3$	$\widehat{\mathcal{Q}}$	$\widehat{\overline{\mathcal{Q}}}$	$\widehat{\mathcal{L}}$	$\widehat{\overline{\mathcal{L}}}$
$SU(3)_C$	3	$\bar{3}$	$\bar{3}$	1	1	1	1	1	1	1	1	1	3	$\bar{3}$	1	1
$SU(2)_L$	2	1	1	2	1	1	2	2	1	1	1	1	1	1	1	1
$U(1)_Y$	1/6	-2/3	1/3	-1/2	0	1	1/2	-1/2	0	0	0	0	$Y_\mathcal{Q}$	$-Y_\mathcal{Q}$	$Y_\mathcal{L}$	$-Y_\mathcal{L}$
$U(1)'$	Q'_Q	Q'_U	Q'_D	Q'_L	Q'_N	Q'_E	Q'_{H_u}	Q'_{H_d}	Q'_S	Q'_{S_1}	Q'_{S_2}	Q'_{S_3}	$Q'_\mathcal{Q}$	$Q'_{\overline{\mathcal{Q}}}$	$Q'_\mathcal{L}$	$Q'_{\overline{\mathcal{L}}}$

TABLE I. *Gauge quantum numbers of quark $(\widehat{Q},\widehat{U},\widehat{D})$, lepton $(\widehat{L},\widehat{N},\widehat{E})$, Higgs $(\widehat{H}_u,\widehat{H}_d)$, SM-singlet $(\widehat{S},\widehat{S}_1,\widehat{S}_2,\widehat{S}_3)$, exotic quark $(\widehat{\mathcal{Q}},\widehat{\overline{\mathcal{Q}}})$ and exotic lepton $(\widehat{\mathcal{L}},\widehat{\overline{\mathcal{L}}})$ superfields.*

three $SU(2)_L$ singlet fields $S_i, i = 1, 2, 3$ which acquire large VEVs. All four VEVs of the singlet fields $S, S_{1,2,3}$ contribute to Z' mass. Thus, in this model, Z'/Z mass hierarchy is implemented mainly through the secluded sector of the model.

The superpotential of the model is given by

$$\widehat{W} = h_u\widehat{Q} \cdot \widehat{H}_u\widehat{U} + h_d\widehat{Q} \cdot \widehat{H}_d\widehat{D} + h_e\widehat{L} \cdot \widehat{H}_d\widehat{E} + h_s\widehat{S}\widehat{H}_u \cdot \widehat{H}_d + \frac{1}{M_R}\widehat{S}_1\widehat{L} \cdot \widehat{H}_u\mathbf{h}_\nu\widehat{N} + \bar{h}_s\widehat{S}_1\widehat{S}_2\widehat{S}_3$$
$$+ \sum_{i=1}^{n_\mathcal{Q}} h_Q^i\widehat{S}\widehat{\mathcal{Q}}_i\widehat{\overline{\mathcal{Q}}}_i + \sum_{j=1}^{n_\mathcal{L}} h_L^j\widehat{S}\widehat{\mathcal{L}}_j\widehat{\overline{\mathcal{L}}}_j \tag{1}$$

where the fields entering the equation, together with their quantum numbers are listed in Table I. Here, M_R is a large mass scale and h_ν is the Yukawa coupling responsible for generating neutrino masses.

The $U(1)'$ charges of the fields satisfy a number of conditions arising from phenomenological constraints, as well as from gauge invariance of the model and from the requirement of cancellation of gauge and gravitational anomalies. They are as follows.

The $U(1)'$ charges satisfy $Q'_{H_u} + Q'_{H_d} \neq 0$ to forbid the bare μ term, $Q'_L + Q'_{H_u} + Q'_N \neq 0$ to induce neutrino masses correctly, and $Q'_{S_1} + Q'_{S_2} + Q'_{S_3} = 0$ to correctly generate the $Z - Z'$ mass hierarchy. Gauge invariance of the superpotential implies

$$0 = Q'_S + Q'_{H_u} + Q'_{H_d},$$
$$0 = Q'_Q + Q'_{H_u} + Q'_U,$$
$$0 = Q'_Q + Q'_{H_d} + Q'_D,$$
$$0 = Q'_L + Q'_{H_d} + Q'_E,$$
$$0 = Q'_\mathcal{Q} + Q'_{\overline{\mathcal{Q}}} + Q'_S,$$
$$0 = Q'_\mathcal{L} + Q'_{\overline{\mathcal{L}}} + Q'_S,$$

$$0 = Q'_{S_1} + Q'_L + Q'_{H_u} + Q'_N. \tag{2}$$

For the model to be anomaly-free the $U(1)'$ charges of fields must satisfy

$$0 = 3(2Q'_Q + Q'_U + Q'_D) + n_Q(Q'_Q + Q'_{\bar{Q}}), \tag{3}$$

$$0 = 3(3Q'_Q + Q'_L) + Q'_{H_d} + Q'_{H_u}, \tag{4}$$

$$0 = 3(\frac{1}{6}Q'_Q + \frac{1}{3}Q'_D + \frac{4}{3}Q'_U + \frac{1}{2}Q'_L + Q'_E) + \frac{1}{2}(Q'_{H_d} + Q'_{H_u})$$
$$+ 3n_Q Y_Q^2(Q'_Q + Q'_{\bar{Q}}) + n_{\mathcal{L}} Y_{\mathcal{L}}^2(Q'_{\mathcal{L}} + Q'_{\bar{\mathcal{L}}}), \tag{5}$$

$$0 = 3(6Q'_Q + 3Q'_U + 3Q'_D + 2Q'_L + Q'_E + Q'_N) + 2Q'_{H_d} + 2Q'_{H_u}$$
$$+ Q'_S + Q'_{S_1} + Q'_{S_2} + Q'_{S_3} + 3n_Q(Q'_Q + Q'_{\bar{Q}}) + n_{\mathcal{L}}(Q'_{\mathcal{L}} + Q'_{\bar{\mathcal{L}}}), \tag{6}$$

$$0 = 3(Q'^2_Q + Q'^2_D - 2Q'^2_U - Q'^2_L + Q'^2_E) - Q'^2_{H_d} + Q'^2_{H_u} + 3n_Q Y_Q(Q'^2_Q - Q'^2_{\bar{Q}})$$
$$+ n_{\mathcal{L}} Y_{\mathcal{L}}(Q'^2_{\mathcal{L}} - Q'^2_{\bar{\mathcal{L}}}), \tag{7}$$

$$0 = 3(6Q'^3_Q + 3Q'^3_D + 3Q'^3_U + 2Q'^3_L + Q'^3_E + Q'^3_N) + 2Q'^3_{H_d} + 2Q'^3_{H_u} + Q'^3_S$$
$$+ Q'^3_{S_1} + Q'^3_{S_2} + Q'^3_{S_3} + 3n_Q(Q'^3_Q + Q'^3_{\bar{Q}}) + n_{\mathcal{L}}(Q'^3_{\mathcal{L}} + Q'^3_{\bar{\mathcal{L}}}), \tag{8}$$

which correspond to vanishing of $U(1)'$-$SU(3)_C$-$SU(3)_C$, $U(1)'$-$SU(2)_L$-$SU(2)_L$, $U(1)'$-$U(1)_Y$-$U(1)_Y$, $U(1)'$-graviton-graviton, $U(1)'$-$U(1)'$-$U(1)_Y$, and $U(1)'$-$U(1)'$-$U(1)'$ anomalies, respectively. All these anomaly cancellation conditions are satisfied for a particular pattern of charges and parameters. It is found that the solution to the mixed anomaly constraints requires $n_Q = 3$ color triplet pairs with hypercharge $Y_Q = -1/3$, and $n_{\mathcal{L}} = 5$ singlet pairs with $Y_{\mathcal{L}} = -\sqrt{2/5}$. With these parameter values one obtains the $U(1)'$ model displayed in Table II. The $U(1)'$ charges for Higgs fields in the model are chosen as

$$Q'_S = -Q'_{S_1} = -Q'_{S_2} = \frac{1}{2}Q'_{S_3}, \quad Q'_{H_u} + Q'_{H_d} + Q'_S = 0. \tag{9}$$

Under the conditions above, the supersymmetry breaking soft terms for the secluded sector model are

$$V_{soft} = V^I_{soft} + V^o_{soft} \tag{10}$$

where V^I_{soft} are the allowed $U(1)'$ dimension-2 operators

$$V^I_{soft} = (m^2_{SS_1}SS_1 + m^2_{SS_2}SS_2 + m^2_{S_1 S_2}S_1^\dagger S_2 + h.c.) \tag{11}$$

and V^o_{soft} term is defined as

$$V^o_{soft} = m^2_{H_u}|H_u|^2 + m^2_{H_d}|H_d|^2 + m^2_S|S|^2 + \sum_{i=1}^3 m^2_{S_i}|S_i|^2$$
$$- (A_s h_s S H_u H_d + A_{\bar{s}} \bar{h}_s S_1 S_2 S_3 + h.c.) \tag{12}$$

7

$Q'_{H_u} = -2$	$Q'_{S_2} = -1$	$Q'_D = -1 - x$	$Q'_Q = \frac{4 - 12x - \sqrt{2}\Omega}{18}$
$Q'_{H_d} = 1$	$Q'_{S_3} = 2$	$Q'_L = \frac{1}{3} - 3x$	$Q'_{\overline{Q}} = \frac{-22 + 12x + \sqrt{2}\Omega}{18}$
$Q'_S = 1$	$Q'_Q = x$	$Q'_E = -\frac{4}{3} + 3x$	$Q'_{\mathcal{L}} = \frac{-15 + 13\sqrt{10} - 12\sqrt{10}x + \sqrt{5}\Omega}{30}$
$Q'_{S_1} = -1$	$Q'_U = 2 - x$	$Q'_N = \frac{8}{3} + 3x$	$Q'_{\overline{\mathcal{L}}} = \frac{-15 - 13\sqrt{10} + 12\sqrt{10}x - \sqrt{5}\Omega}{30}$

TABLE II. *A set of $U(1)'$ charges satisfying all gauge invariance and anomaly cancellation conditions. The charge of the quark doublet $\widehat{Q}$ is left free, and for simplicity $\Omega(x) = \sqrt{241 + 708x + 612x^2}$ is introduced.*

We set $m^2_{S_1 S_2} = 0$ as only two of the S_i fields are needed to break the global $U(1)$ symmetries. To insure that the potential is not bounded from below, we require

$$m^2_S + m^2_{S_1} + 2m^2_{SS_1} > 0\,,$$
$$m^2_S + m^2_{S_2} + 2m^2_{SS_2} > 0. \tag{13}$$

In the model, the charge of the quark doublet $\widehat{Q}$ is kept as a free parameter after the normalization $Q'_{H_u} = -2$, $Q'_{H_d} = 1$, $Q'_S = 1$, $Q'_{S_1} = -1$, $Q'_{S_2} = -1$, $Q'_{S_3} = 2$.

In this model the left and right sneutrinos mix, and the mixing matrix can in general be expressed as

$$\mathcal{L}^{\widetilde{\nu}}_m = -\sum_{i,j=1}^{3} (\widetilde{\nu}_L^{i*} \widetilde{\nu}_R^{j*}) \begin{pmatrix} m^2_{\widetilde{\nu}^i_{LL}} & m^2_{\widetilde{\nu}^{ij}_{LR}} \\ m^2_{\widetilde{\nu}^{ij}_{RL}} & m^2_{\widetilde{\nu}^j_{RR}} \end{pmatrix} \begin{pmatrix} \widetilde{\nu}_L^i \\ \widetilde{\nu}_R^j \end{pmatrix}, \tag{14}$$

where i, j are the flavor indices and the matrix elements are given by

$$m^2_{\widetilde{\nu}^i_{LL}} = M^2_{L_i} + (\mathbf{m}^{ii}_\nu)^2 + \frac{1}{4}(g_Y^2 Y_L - \frac{g^2}{2})(\langle H_u^0 \rangle^2 - \langle H_d^0 \rangle^2)$$
$$+ \frac{1}{2} g_{Y'}^2 Q'_L (Q'_{H_u} \langle H_u^0 \rangle^2 + Q'_{H_d} \langle H_d^0 \rangle^2 + Q'_S \langle S \rangle^2 \rho_s)$$

$$m^2_{\widetilde{\nu}^j_{RR}} = M^2_{N_j} + (\mathbf{m}^{ii}_\nu)^2 + \frac{1}{4} g_Y^2 Y_N (\langle H_u^0 \rangle^2 - \langle H_d^0 \rangle^2)$$
$$+ \frac{1}{2} g_{Y'}^2 Q'_N (Q'_{H_u} \langle H_u^0 \rangle^2 + Q'_{H_d} \langle H_d^0 \rangle^2 + Q'_S \langle S \rangle^2 \rho_s)$$

$$m^2_{\widetilde{\nu}^{ij}_{LR}} = (m^2_{\widetilde{\nu}^{ij}_{RL}})^* = \mathbf{m}^{ij}_\nu \left[A^*_{\nu_i} + \frac{\mu}{\tan \beta} + \frac{\bar{h}_s \langle S_2 \rangle \langle S_3 \rangle}{\sqrt{2} \langle S_1 \rangle} \right]. \tag{15}$$

Here $M^2_{L_i}$ and $M^2_{N_i}$ are soft mass terms and A_{ν_i} are trilinear couplings (assumed flavor-diagonal). Dirac neutrino masses $\mathbf{m}_\nu$, the μ parameter and ρ_s in the equations above are expressed as

$$\mathbf{m}_\nu = \frac{1}{M_R} \langle S_1 \rangle \langle H_u^0 \rangle \mathbf{h}_\nu \equiv \mathbf{Y}_\nu \left(\langle H_u^0 \rangle / \sin \beta \right), \quad \mu = \frac{h_s \langle S \rangle}{\sqrt{2}}, \quad \rho_s = 1 + \frac{\sum_{i=1}^{3} Q'_{S_i} v^2_{s_i}}{Q'_S v^2_s}. \tag{16}$$

In this model, neutrino masses are chosen to be Dirac-type. The effective neutrino Yukawa coupling $\mathbf{Y}_\nu$ leads to neutrino masses in agreement with the experiment. Numerically, we obtain [8]

$$|\mathbf{Y}_\nu| \simeq 3 \times 10^{-13} \left(\frac{|m_\nu|^2}{2.8 \times 10^{-3} \text{ eV}^2} \right)^{1/2}. \tag{17}$$

III. MSSM VS. $U(1)'$ AT THE LHC ENERGIES

A. Parameter Space and Relic Density

Motivated by the fact that the scalar neutrino LSP can in principle explain the WMAP data as well as excess positron flux measured by various satellite experiments [8], we analyze the model further by investigating the production and decay mechanism of the scalar neutrinos at LHC.

The model we consider here, the secluded-$U(1)'$ with right-handed neutrinos, has some advantages over the so-called the minimal $U(1)'$ where only one additional scalar field is introduced. The squark phenomenology in this minimal $U(1)'$ model has been explored in Ref. [15] where there is difficulty with inducing a small μ_{eff} while satisfying the Z' mass bound, which is around 1 TeV. This is because both μ_{eff} and $m_{Z'}$ are proportional to the vacuum expectation value of the additional scalar field S. One needs three additional scalars to ameliorate the picture the VEVs of the new scalars are kept large large. This is one motivation for the secluded $U(1)'$ model. For further details of the model, see [7].
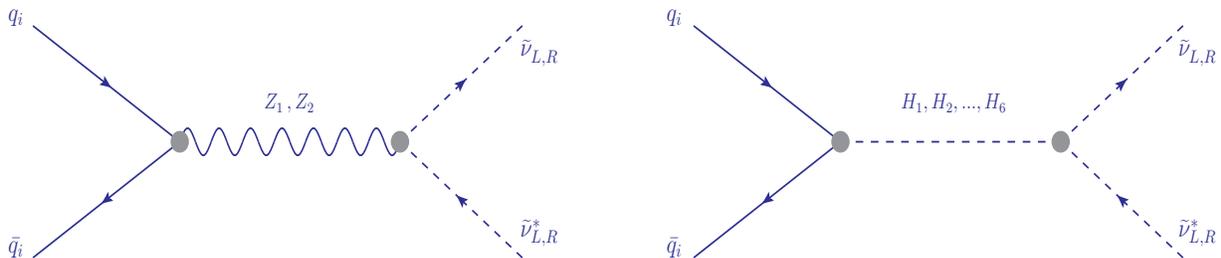
FIG. 1. *The Feynman diagrams for the production of the scalar neutrinos in the secluded-$U(1)'$ model. $H_i, i = 1, ..., 6$ are the CP-even physical Higgs bosons.*

The Feynman diagrams contributing to the hard production of scalar neutrinos are given in Fig 1. For simplicity we neglect the mixing between Z (the Z boson of the SM) and Z' in

the numerical analysis so that $Z_1 \equiv Z$ and $Z_2 \equiv Z'$. In addition to Z' exchange (left-handed diagram), all CP-even Higgs bosons contribute to the process in the s-channel (right-handed diagram).

Once the scalar neutrinos are produced, they will decay. The decay pattern strictly depends on scenario chosen for the free parameters. Since we are interested in rather light scalar neutrinos (assuming low-energy SUSY exits), we prefer to choose MSSM-like Low Mass (LM) scenarios [9]. Battaglia *et. al* have proposed updated post-WMAP benchmark points for the constrained MSSM [10] modifying earlier proposal [11], and we include these points in Table III.

To compare our results with MSSM predictions, we choose three low-mass MSSM scenarios (benchmark points), namely LM1, LM2 and LM6, from the low mass scenarios of MSUGRA and use `Softsusy` package [16] to generate the MSSM spectrum. In the secluded $U(1)'$ we choose LM-like scenarios, denoted as LM1′, LM2′ and LM6′ by keeping the overlapping parameters the same and fixing the additional parameters to agree with phenomenological constraints on masses. The input parameters for LM1, LM2 and LM6 for MSSM as well as their corresponding prime versions for the secluded $U(1)'$ are given in Table III. As seen from Table III, the VEVs of the additional scalars (S_1, S_2 and S_3) $v_{s_i}, i = 1, 2, 3$ are taken above the TeV scale so that the Z' mass bound is satisfied no matter what the VEV of the scalar field S is chosen. In fact, for convenience, the parameters μ_{eff} and h_s are taken as free parameters and the VEV of S are determined accordingly using the relation given in Eq. (16). From Table IV it is seen that the scalar neutrino masses are rather light. The left-handed sneutrinos masses are varying in the 168 GeV-287 GeV range while the right-handed ones are in the 412 GeV-704 GeV depending on the LM scenario as well as on the flavor of the scalar neutrino. The right-handed scalar neutrinos are heavier, showing the same pattern as in the neutrino sector. With these chosen masses we can foresee that the production cross section for the left-handed sneutrinos will dominate the one for the right-handed ones.

The validity of the MSSM scenarios LM1, LM2 and LM6 has been confronted with both the LEP and Tevatron data. There will be no contributions to the LEP observables from our LMX′, X = 1, 2, 6 scenarios since the lightest Higgs boson mass in the model is 218 GeV, which is already above the LEP energy. For the Tevatron case, however, one needs do a more careful analysis. Nevertheless, as the LMX′ scenarios aim to be consistent with

Parameters	MSSM			U(1)$'$		
	LM1	LM2	LM6	LM1$'$	LM2$'$	LM6$'$
$\text{sign}(\mu)$	+	+	+	+	+	+
$\tan\beta$	10	35	10	10	35	10
Q'_Q	–	–	–	-2	-2	-2
$\mu\,(\mu_{eff})$	373	506	583	373	506	583
h_ν	–	–	–	1	1	1
h_s	–	–	–	0.5	0.7	0.7
$\bar{h}_s$	–	–	–	0.75	0.75	0.70
A_s	–	–	–	200	200	200
$A_{\bar{s}}$	–	–	–	100	100	100
v_{s_1}	–	–	–	1450	1350	1600
v_{s_2}	–	–	–	1250	1250	1450
v_{s_3}	–	–	–	1150	1100	1300
$R_{Y'}$	–	–	–	49.4	45	42
$M_{\tilde{\nu}_{eR}}$	–	–	–	400	500	600
$M_{\tilde{\nu}_{\mu R}}$	–	–	–	450	550	650
$M_{\tilde{\nu}_{\tau R}}$	–	–	–	500	600	700
M_1	98	139	159	98	139	159
M_2	189	266	303	189	266	303
M_3	630	871	989	630	871	989
M_{L_1}	181	295	284	199	295	284
M_{E_1}	110	218	171	121	218	171
M_{Q_1}	586	821	916	586	821	916
M_{U_1}	569	797	888	569	797	888
M_{D_1}	567	795	885	567	795	885
M_{L_2}	181	295	284	199	295	284
M_{E_2}	110	218	171	121	218	171
M_{Q_2}	586	821	916	586	821	916
M_{U_2}	569	797	888	569	797	888
M_{D_2}	567	795	885	567	795	885
M_{L_3}	180	283	284	198	283	284
M_{E_3}	108	182	168	121	182	168
M_{Q_3}	538	731	842	538	731	842
M_{U_3}	467	652	729	467	652	729
M_{D_3}	563	748	879	563	748	879
$M^2_{SS_{1,2}}$	–	–	–	-2×10^6	-2×10^6	-2×10^6
A_t	-517	-698	-806	-517	-698	-806
A_b	-791	-960	-1224	-791	-960	-1224
A_τ	-159	-139	-251	-159	-139	-251

TABLE III. *The scenarios (benchmark points) LM1, LM2, and LM6 (for the MSSM i. e. minimal supergravity), and LM1$'$, LM2$'$ and LM6$'$ (for the U$(1)'$ model). The unprimed LMX and primed LMX$'$ benchmark points similar mass spectra. Parameter $R_{Y'}$ is defined in Appendix C.*

Masses	MSSM			U(1)′		
	LM1	LM2	LM6	LM1′	LM2′	LM6′
$m_{Z'}$	–	–	–	1476	1418	1661
$m_{\tilde{\chi}_1^0}$	96	141	161	96	63	79
$m_{\tilde{\chi}_2^0}$	178	264	302	99	138	158
$m_{\tilde{\chi}_3^0}$	340	448	513	177	258	295
$m_{\tilde{\chi}_4^0}$	360	462	529	356	443	425
$m_{\tilde{\chi}_5^0}$	–	–	–	392	527	603
$m_{\tilde{\chi}_6^0}$	–	–	–	412	536	609
$m_{\tilde{\chi}_7^0}$	–	–	–	633	593	657
$m_{\tilde{\chi}_8^0}$	–	–	–	1364	1311	1438
$m_{\tilde{\chi}_9^0}$	–	–	–	5312	6592	7110
$m_{\tilde{\chi}_1^\pm}$	177	264	303	174	256	293
$m_{\tilde{\chi}_2^\pm}$	362	466	532	397	523	598
$m_{\tilde{e}_L}$	186	298	287	155	248	271
$m_{\tilde{e}_R}$	120	223	178	193	285	206
$m_{\tilde{\mu}_L}$	186	298	287	155	248	271
$m_{\tilde{\mu}_R}$	120	223	178	193	285	206
$m_{\tilde{\tau}_1}$	111	146	171	144	168	195
$m_{\tilde{\tau}_2}$	190	309	289	200	305	276
$m_{\tilde{\nu}_e}$	168	287	276	133	235	259
$m_{\tilde{\nu}_\mu}$	168	287	276	133	235	259
$m_{\tilde{\nu}_\tau}$	168	274	275	132	219	258
$m_{\tilde{\nu}_{e_R}}$	–	–	–	412	514	604
$m_{\tilde{\nu}_{\mu_R}}$	–	–	–	460	563	654
$m_{\tilde{\nu}_{\tau_R}}$	–	–	–	509	612	704
$m_{H_1^0}$	109	112	112	218	252	238
$m_{H_2^0}$	371	423	576	780	807	735
$m_{H_3^0}$	–	–	–	852	870	942
$m_{H_4^0}$	–	–	–	884	1198	1089
$m_{H_5^0}$	–	–	–	1251	1883	1339
$m_{H_6^0}$	–	–	–	2789	2770	2844
$m_{A_1^0}$	371	423	576	418	412	431
$m_{A_2^0}$	–	–	–	868	1256	1085
$m_{A_3^0}$	–	–	–	1257	1883	1246
$m_{A_4^0}$	–	–	–	2591	2586	2599
$m_{H^\pm}$	380	431	581	867	1881	1081

TABLE IV. *The complete mass spectra of the benchmark points (scenarios) given in Table III for both MSSM and the secluded $U(1)'$.*

the corresponding MSSM scenarios, in the limit where the extra $U(1)'$ particles decouple, we expect consistency with the Tevatron data. To verify this point, we used the package `HiggsBounds` [17], which yields results for any arbitrary Higgs sector.

Observables	MSSM			$U(1)'$		
	LM1	LM2	LM6	LM1$'$	LM2$'$	LM6$'$
$\sigma(\text{pp} \to \tilde{\nu}_{e_R}\tilde{\nu}_{e_R}^*)$/fb	-	-	-	80.5	67.8	29.1
$\sigma(\text{pp} \to \tilde{\nu}_{\mu_R}\tilde{\nu}_{\mu_R}^*)$/fb	-	-	-	66.7	55.1	24.0
$\sigma(\text{pp} \to \tilde{\nu}_{\tau_R}\tilde{\nu}_{\tau_R}^*)$/fb	-	-	-	54.9	44.6	19.7
$\sigma(\text{pp} \to \tilde{\nu}_{\ell_L}\tilde{\nu}_{\ell_L}^*)$/fb	36.7	4.1	5.3	887.6	734.0	371.9
$\sigma(\text{pp} \to \tilde{\nu}_{\tau_L}\tilde{\nu}_{\tau_L}^*)$/fb	37.2	4.9	5.3	890.7	778.7	373.1
$\sigma_{\text{TOT}}(\text{pp} \to \tilde{\nu}_i\tilde{\nu}_i^*)$/fb	110.6	13.1	15.9	2868.0	2414.2	1189
$\Omega_{\text{DM}}h^2$	0.120	0.120	0.120	0.115	0.109	0.100

TABLE V. *The production cross section and the relic density Ω_{DM} values for the LM scenarios considered in the paper.*

The production cross sections for the scattering $pp \to \tilde{\nu}_{\ell_{L,R}}\tilde{\nu}_{\ell_{L,R}}^*$ processes are listed in Table V, for both MSSM and the secluded $U(1)'$ model. The values were obtained implementing the secluded $U(1)'$ model into `CalcHEP` [18] with the help of `LanHEP` [19]. The parton distributions in the proton have been parametrized by using `CTEQ6M` of `LHAPDF` [20]. The MSSM total cross sections (including the three scalar neutrino flavors) are in the range of 4 to 110 fb while in the secluded $U(1)'$ model they are varying between 1.1 pb to 2.6 pb. The new right-handed sneutrino cross sections in the secluded $U(1)'$ model are about 10 times smaller than the cross sections for their left-handed counterparts, and are in the range of 20 fb to 80 fb.

In Table V, we also included the relic density of the dark matter for all six scenarios. This calculation is straightforward using the `Micromegas` package [21], once we include the model files from `CalcHEP`. All the numbers are within the 1σ range of the WMAP result [22] which can be given with those from the Sloan Digital Sky Survey [12]

$$\Omega_{DM}h^2 = 0.111^{+0.011}_{-0.015}. \tag{18}$$

We note that the relic density of the dark matter $\Omega_{\text{DM}}h^2$ is very sensitive to the free parameter
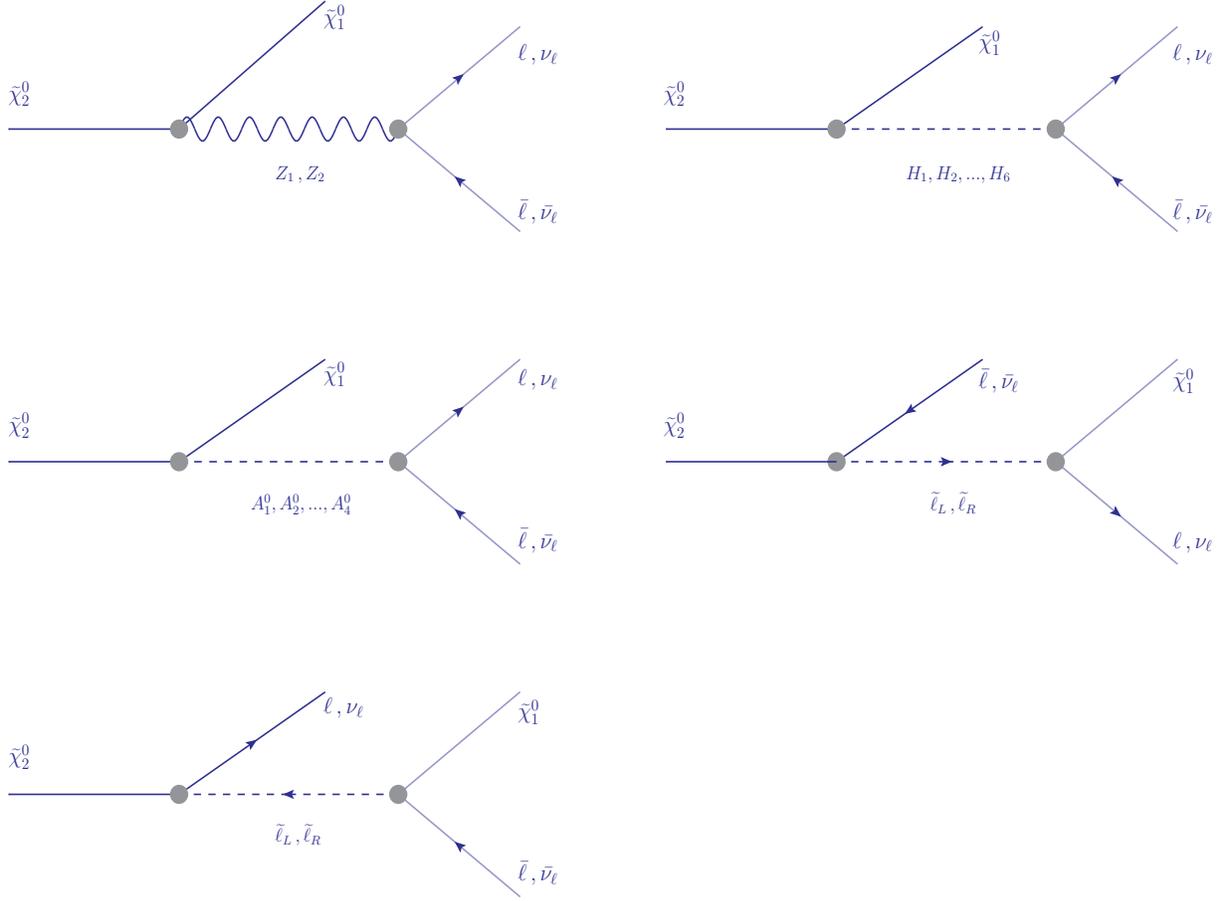
FIG. 2. *The Feynman diagrams for the three-body decay channels of the next-to-LSP $\widetilde{\chi}_2^0$ in the secluded-U(1)$'$ model. Here $H_i, i = 1, ..., 6$ are the CP-even physical Higgs bosons while $A_i^0, i = 1, ..., 4$ are CP-odd ones.*

$R_{Y'}$ listed in Table III which varies between 42 to 50. It's defined (see also Appendix C) as the ratio between bare $U(1)$ gaugino masses

$$R_{Y'} \equiv M_{\widetilde{Y}'}/M_{\widetilde{Y}}$$

where $M_{\widetilde{Y}}$ and $M_{\widetilde{Y}'}$ are the Bino and Bino$'$ mass parameters appearing in the 9×9 neutralino mixing matrix. More details are given in Appendix C. In Table IV the Lightest Supersymmetric Particle (LSP) is the lightest neutralino $\widetilde{\chi}_1^0$ with masses 96 GeV, 63 GeV and 79 GeV for the LM1$'$, LM2$'$ and LM6$'$ scenarios, respectively. The next-to-lightest supersymmetric particle is $\widetilde{\chi}_2^0$ with masses 99 GeV, 138 GeV and 158 GeV, respectively. For such a spectrum, there will be no kinematically available two-body decays for the $\widetilde{\chi}_2^0$, so that three-body channels need to be considered. The three-body decay modes relevant to

14

the analysis here are given in Fig. 2. These decay modes will be considered in the LHC simulation but not the relic density calculation, as they give negligible contributions. The sizable contributions to the relic density are for the LM1′ scenario

- $\widetilde{\chi}_1^0 \widetilde{\chi}_2^0 \to \tau^- \tau^+$ (15%)

- $\widetilde{\chi}_2^0 \widetilde{\chi}_2^0 \to \tau^- \tau^+$ (13%)

- $\widetilde{\chi}_1^0 \widetilde{\chi}_2^0 \to e^- e^+ / \mu^- \mu^+$ (8% for each channel)

- $\widetilde{\chi}_2^0 \widetilde{\chi}_2^0 \to e^- e^+ / \mu^- \mu^+$ (8% for each channel)

- $\widetilde{\chi}_2^0 \widetilde{\chi}_2^0 \to \nu_l \bar{\nu}_l \,, l = e, \mu, \tau$ (5% for each channel)

- $\widetilde{\chi}_1^0 \widetilde{\chi}_1^0 \to \tau^- \tau^+$ (5%)

- $\widetilde{\chi}_1^0 \widetilde{\chi}_1^0 \to e^- e^+ / \mu^- \mu^+$ (3% for each channel)

- $\widetilde{\chi}_1^0 \widetilde{\chi}_2^0 \to \nu_l \bar{\nu}_l \,, l = e, \mu, \tau$ (3% for each channel)

- $\widetilde{\chi}_1^0 \widetilde{\chi}_2^0 \to W^- W^+$ (2%)

In the LM2′(LM6′) only $\widetilde{\chi}_1^0 \widetilde{\chi}_1^0$ annihilation contributes to the relic density of the dark matter as follows

- $\widetilde{\chi}_1^0 \widetilde{\chi}_1^0 \to \tau^- \tau^+$ (75% (38%))

- $\widetilde{\chi}_1^0 \widetilde{\chi}_1^0 \to \mu^- \mu^+$ (8% (26%))

- $\widetilde{\chi}_1^0 \widetilde{\chi}_1^0 \to e^- e^+$ (8% (26%))

- $\widetilde{\chi}_1^0 \widetilde{\chi}_1^0 \to b\bar{b}$ (3% (%1))

- $\widetilde{\chi}_1^0 \widetilde{\chi}_1^0 \to \nu_\tau \bar{\nu}_\tau$ (1% (3%))

- $\widetilde{\chi}_1^0 \widetilde{\chi}_1^0 \to \nu_l \bar{\nu}_l \,, l = e, \mu$ (0% (3%))

- $\widetilde{\chi}_1^0 \widetilde{\chi}_1^0 \to d\bar{d} / s\bar{s}$ (1% (0%))

Contributions from the $\widetilde{\chi}_2^0 \widetilde{\chi}_2^0$ or $\widetilde{\chi}_1^0 \widetilde{\chi}_2^0$ annihilations for the $\widetilde{\chi}_1^0$ scenario are due to the fact that $\widetilde{\chi}_1^0$ and $\widetilde{\chi}_2^0$ are almost degenerate in mass and since the two-body decay channel limit is used in `Micromegas`, $\widetilde{\chi}_2^0$ acts very similar to $\widetilde{\chi}_1^0$. There is no sizable contributions from $\widetilde{\chi}_2^0$ in the other two scenario since $\widetilde{\chi}_2^0$ is much heavier. The bino, wino, higgsino and singlino compositions of the neutralinos for the scenarios LM1′, LM2′ and LM6′ are given in Table VI in Appendix D. The LSP $\widetilde{\chi}_1^0$ is mainly bino for LM1′ but mostly singlino ($\widetilde{S}$) for LM2′ and LM6′ (94.2% and 93.6%, respectively, for the two scenarios). The situation is reversed for the next-to-LSP, $\widetilde{\chi}_2^0$.

B.   The LHC Signals

After discussing the chosen scenarios and the details of the relic density calculation of the dark matter, we proceed to discuss the signals at LHC from scalar neutrino production processes. To determine and classify all possible signals for the scenarios LM1′, LM2′ and LM6′, we need to look at the decay topology of the scalar neutrinos.

Since we include MSSM scenarios LM1, LM2 and LM6 for comparison purposes, we first outline the main decay modes governing the decay channels. The left-handed scalar neutrinos $\widetilde{\nu}_{\ell_L}$ decay to $\nu_\ell \widetilde{\chi}_1^0$ with about 100% branching ratio for the LM1 and LM6, since all the other neutralinos are heavier than the scalar neutrinos. The picture is a bit more complicated for the LM2 where $\widetilde{\nu}_{\ell_L}, \ell = e, \mu$ decay to $\nu_\ell \widetilde{\chi}_1^0$ (71%), $\ell \widetilde{\chi}_1^\pm$ (20%) and $\nu_\ell \widetilde{\chi}_2^0$ (8.8%). For the $\widetilde{\nu}_{\tau_L}$, the branching decay ratios are $W \widetilde{\tau}_1$ (61.5%), $\nu_\tau \widetilde{\chi}_1^0$ (34.2%), $\tau \widetilde{\chi}_1^\pm$ (3%) and $\nu_\tau \widetilde{\chi}_2^0$ (1.3%). Further in the decay chain $\widetilde{\chi}_2^0$ decays mainly to $\tau \widetilde{\tau}_1 / \bar{\tau} \widetilde{\tau}_1^*$ (48% for each channel), and the chargino $\widetilde{\chi}_1^\pm to \nu_\tau \widetilde{\tau}_1$ (with 95.4% branching ratio) and $W \widetilde{\chi}_1^0$ (4.6% branching ratio).

In the secluded $U(1)'$ model, the decay modes of the scalar neutrinos with more than 1% branching ratio are, for the scenarios LM1′/LM2′/LM6′

- $\widetilde{\nu}_{\ell_L} (\widetilde{\nu}_{\ell_R}) \to \nu_\ell \widetilde{\chi}_1^0$,   8.6% (0%) / 91.7% (84.8%) / 93.2% (65.7%)

- $\widetilde{\nu}_{\ell_L} (\widetilde{\nu}_{\ell_R}) \to \nu_\ell \widetilde{\chi}_2^0$,   91.4% (90.6%) / 8.3% (0%) / 6.8% (0%)

- $\widetilde{\nu}_{\ell_L} (\widetilde{\nu}_{\ell_R}) \to \nu_\ell \widetilde{\chi}_4^0$,   0% (8.8%) / 0% (14.8%) / 0% (34.1%)

There will be further decays of $\widetilde{\chi}_2^0$ and $\widetilde{\chi}_4^0$ in the chain. It is better to consider $\widetilde{\chi}_4^0$ first. Again in the same notation (LM1′/LM2′/LM6′) it decays as

- $\widetilde{\chi}_4^0 \to \tau \, \widetilde{\tau}_1^* \; (\tau \, \widetilde{\tau}_2^*)$,   6.5% (4.9%) / 9.1% (3.7%) / 8.6% (3.9%)

- $\widetilde{\chi}_4^0 \to \ell \, \widetilde{\ell}_L^* \; (\ell \, \widetilde{\ell}_R^*)$,   6.0% (5.3%) / 5.2% (5.0%) / 4.0% (8.3%)

- $\widetilde{\chi}_4^0 \to \nu_\ell \, \widetilde{\nu}_{\ell_L}^* \; (\nu_\tau \, \widetilde{\nu}_{\tau_L}^*)$,   5.2% (5.2%) / 5.4% (5.9%) / 4.2% (4.3%)

where $\ell = e, \mu$ and the conjugated decay modes are not listed. Then the decay modes of the scalar leptons for $\ell = e, \mu^*$ are

- $\widetilde{\ell}_L \to \ell \, \widetilde{\chi}_1^0 \; (\ell \, \widetilde{\chi}_2^0)$,   6.7% (93.3%) / 90.1% (9.9%) / 92.6% (7.4%)

- $\widetilde{\ell}_R \to \ell \, \widetilde{\chi}_1^0 \; (\ell \, \widetilde{\chi}_2^0)$,   20% (80%) / 71.6% (28.4%) / 89.7% (10.3%)

As can be seen from the above decay patterns, each decay ends up with either an LSP $\widetilde{\chi}_1^0$ or next-to-LSP particle $\widetilde{\chi}_2^0$. As mentioned earlier, $\widetilde{\chi}_2^0$ cannot decay into two-body but instead must undergo the one of the three-body decays given in Fig. 2. The relative ratios are[†] given in the (LM1′/LM2′/LM6′) order as

- $\widetilde{\chi}_2^0 \to \nu_\ell \, \bar{\nu}_\ell \, (\nu_\tau \, \bar{\nu}_\tau) \, \widetilde{\chi}_1^0$,   24% (24%) / 4.5% (6.3%) / 1.8% (1.8%)

- $\widetilde{\chi}_2^0 \to \ell^+ \, \ell^- \, (\tau^+ \, \tau^-) \, \widetilde{\chi}_1^0$,   14% (0%) / 10.8% (63%) / 28.7% (37%)

In the light of these decay patterns, there are mainly three types of signal: (1) $0\ell + \not{E}_T$, (2) $2\ell + \not{E}_T$ and (3) $4\ell + \not{E}_T$. It is in fact also possible to produce signals with six or eight leptons but the probability is very suppressed thus we ignore such signals. Therefore, in the rest of this section we discuss these three signals at LHC. Predictions from MSSM will be included as well. In MSSM there is no the $4\ell + \not{E}_T$ type of signal in MSSM for the LM1 and LM2 and LM2 scenarios. The $2\ell + \not{E}_T$ signal is possible through chargino $\widetilde{\chi}_1^\pm$ decay.

The usual concern is the possible background for the signals from the SM. For the $0\ell + \not{E}_T$ mode, the background will come from the Drell-Yan (D-Y), $pp \to \nu_\ell \bar{\nu}_\ell$, and $pp \to ZZ$ where each of Z decays invisibly. Since the D-Y has a huge cross section, some cuts need to be implemented. In the $2\ell + \not{E}_T$ case, in addition to the D-Y and ZZ production (where one of the Z decays leptonicaly), there is $W^+ W^-$ production. In principle there could be contributions from the $t\bar{t}$ with jet veto, but we ignore such possibility since the b-jets are going to be quite energetic and can be tagged. The process $pp \to ZZ \to 4\ell$ can be the

---

[*] We discard $\ell = \tau$ case since such a pattern ends up with a τ lepton in the final state. We concentrate only on the first two generations of the charged leptons.

[†] Note that the $\tau^- \tau^-$ channel is not kinematically open for the LM1′ scenario.

background for the $4\ell + \not{E}_T$ decay mode. However, a simple $\not{E}_T$ cut would eliminate events from the SM process $pp \to ZZ \to 4\ell$. We confirmed this with our event simulation.

At the first stage, the following basic cuts are applied to suppress the SM background. It is required that, whenever relevant,

- Each isolated charged lepton (electron or muon) has a transverse momentum $p_T(\ell) > 15\,\text{GeV}$.

- The missing transverse energy satisfies $\not{E}_T > 100\,\text{GeV}$.

- The leptons are constrained to be in the central barrel region of the detector by forcing the pseudorapidity $|\eta| < 2$.

- The cone size between two charged lepton $\Delta R_{\ell\ell}$ is at least 0.4. Here $\Delta R_{\ell\ell} = (\Delta\eta^2 + \Delta\phi^2)^{1/2}$ defined in the pseudorapidity-azimuthal angle plane.

As mention above, a missing transverse energy cut $\not{E}_T > 100\,\text{GeV}$ practically gets rid of the SM background for the $4\ell + \not{E}_T$ signal, which is now considered background free. For the $4\ell + \not{E}_T$ signal, in order to get enough statistics after the cuts (as much less number of events pass the cuts as compared of the other two signals), we relaxed the some of the above cuts. We use $p_T(\ell) > 5\,\text{GeV}$ and $\Delta R_{\ell\ell} > 0.2$ for the analysis of this signal.

With the above cuts, the SM background is still larger than the signals $0\ell + \not{E}_T$ and $2\ell + \not{E}_T$. The D-Y and W^+W^- dominate the ZZ cross section and they are all well above the signal for $\not{E}_T < 500\,\text{GeV}$. Such background domination happens in various other distributions in most part of the region. There is no point to present these figures. Instead we need to find a better way to handle the background. After examining the results at the first stage, we decided to use E_T^{sum}, also known as the effective mass m_{eff} in literature. This variable could be helpful in reducing the backgrounds while keeping most of the signal events especially if we use a suitable value for the cuts. E_T^{sum} is defined as the scalar sum of the lepton transverse momenta and the missing transverse energy

$$E_T^{\text{sum}} \equiv m_{\text{eff}} = \sum_\ell |p_T(\ell)| + \not{E}_T. \tag{19}$$

where the missing transverse energy $\not{E}_T$ is the sum of the total x and y components of the momenta in quadratures. Since it has been observed that the signal processes lead to mostly high m_{eff} (or E_T^{sum}) distributions, a cut on m_{eff} would substantially reduce the background.

18

Thus, as a second stage for the cuts $m_{\text{eff}} = E_T^{\text{sum}} > 750\,\text{GeV}$ has been employed (but only for the $0\ell + \not{E}_T$ and $2\ell + \not{E}_T$ cases.)

Global inclusive variables like $\not{E}_T$ and E_T^{sum} are used to estimate the mass scalar of the parent particles produced in the hard scattering (thus estimating the scale of the new physics). In a recent paper by Konar $et\ al.$ [23], a new global inclusive variable, called $\hat{s}_{\text{min}}^{1/2}$, is proposed as an alternative. For SUSY models with R parity conservation, the decay chain always ends with an LSP, which is left undetected at the collider. This makes mass reconstruction procedure almost impossible, especially if there are more than one LSP (there are at least have two LSPs in the final state). Without going into extensive details of the signal, there is an easy way to approach guessing the scale of the new physics through the parameter $\hat{s}_{\text{min}}^{1/2}$. It is defined as [23]

$$\hat{s}_{\text{min}}^{1/2} = \sqrt{E^2 - P_z^2} + \sqrt{\not{E}_T^2 + M_{\text{invisible}}^2} \tag{20}$$

where E is the total calorimeter energy, $\vec{P}$ is the total $visible$ momentum and $M_{\text{invisible}}$ is the total mass of all invisible particles produced in each event, which is the only unknown. All the others variables can be measured at the detector. Hence $\hat{s}_{\text{min}}^{1/2}(M_{\text{invisible}})$ is the variable to consider. The $peak$ of the $\hat{s}_{\text{min}}^{1/2}$ distribution is associated with the mass threshold of the parent particles originated from the hard scattering. Of course, an estimation needs to be done for the total invisible mass $M_{\text{invisible}}$. In most of the cases the $\hat{s}_{\text{min}}^{1/2}(0)$ gives a pretty good idea about the masses of the parent particles. It is shown that the method works better for signals with fewer invisible particles and/or more visible particles. It also works better with higher SUSY scales where Initial State Radiations (ISR) are less significant. We include some figures for $\hat{s}_{\text{min}}^{1/2}(0)$ in the $0\ell + \not{E}_T$ as well as $4\ell + \not{E}_T$ signal.

The events are generated at the partonic level with `CalcHEP` [18] and passed to `Pythia` [24] with the use of `CalcHEP-Pythia` interface for hadronization and cuts. We simulated 4×10^6 events for the $0\ell + \not{E}_T$, $2\ell + \not{E}_T$ and $4\ell + \not{E}_T$ signals. Since the relative number of events in each signal turns out to be proportional to the relevant branching ratio combination, the number of events can be simply weighed by $w = \sigma(pp \to \tilde{\nu}_\ell \tilde{\nu}_\ell^*) \times \mathcal{L}/N_{\text{tot}}$ where $\mathcal{L}$ is the integrated luminosity and N_{tot} is the total number of event generated. We set $\mathcal{L} = 100\ \text{fb}^{-1}$, the ultimate goal that is expected at the LHC. Even though the current reach of LHC center of mass energy is $7\,\text{TeV}$, we use $14\,\text{TeV}$ in the numerical study, which maximizes the reach in the parameter space.
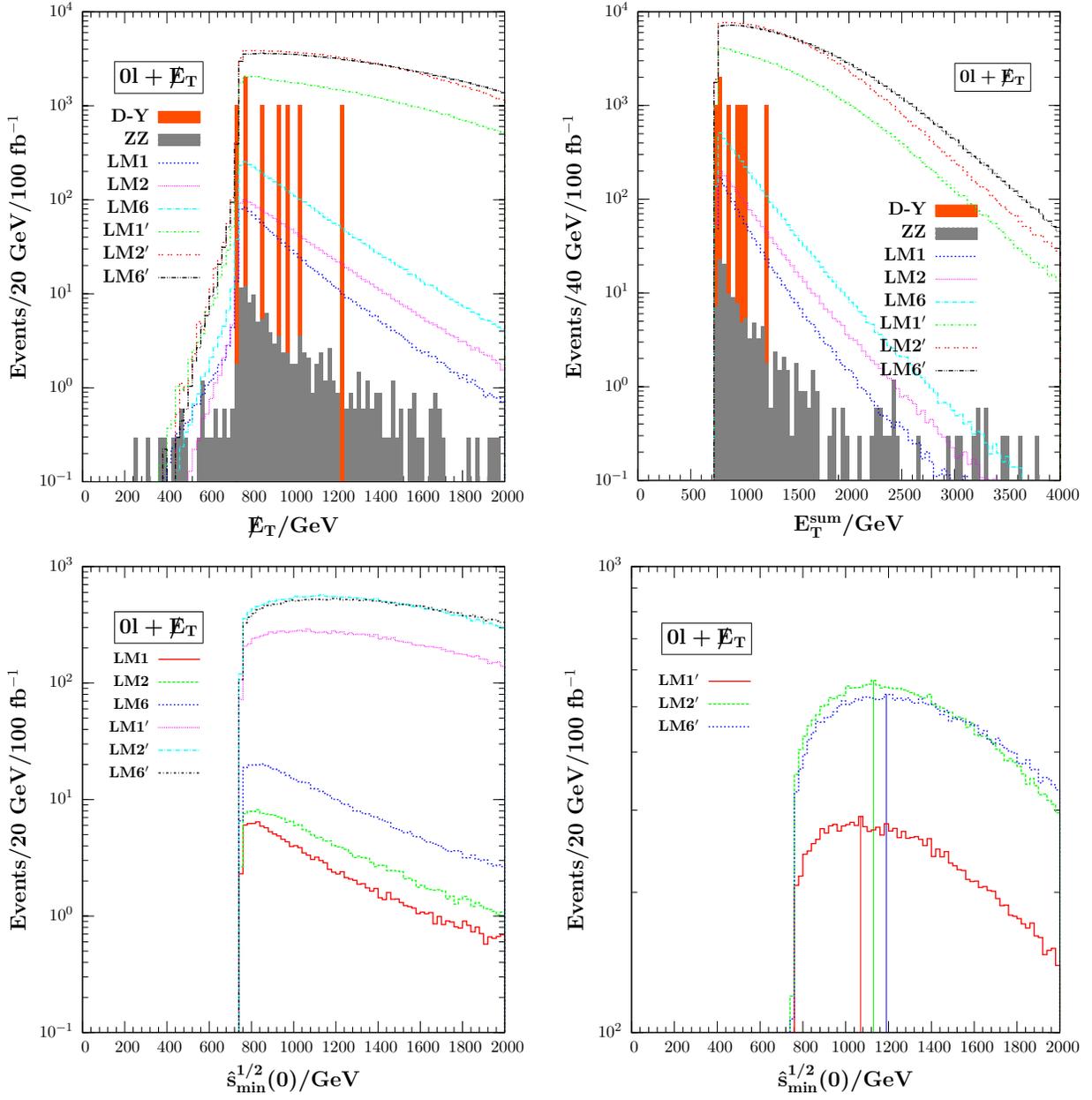
FIG. 3. *The $\not{E}_T$, E_T^{sum}, and $\hat{s}_{\text{min}}^{1/2}(0)$ distributions of the $0\ell+\not{E}_T$ signal at $14\,\text{TeV}$ with integrated luminosity $\mathcal{L} = 100\,\text{ fb}^{-1}$, for the three scenarios in both MSSM and the secluded $U(1)'$ model.*

1. *The Missing Energy Signal: $0\ell+\not{E}_T$*

The distributions of $\not{E}_T$, E_T^{sum}, and $\hat{s}_{\text{min}}^{1/2}(0)$ are depicted in Fig. 3 for the three scenarios LM1′, LM2′ and LM6′ as well as the three benchmarks for the MSSM. In general the LM6′ scenario has the largest event pass the cuts, with similar results for the LM2′, while the LM1′ has the lowest. In fact about 80% of the events pass the cuts in LM2′ and LM6′

20

but only 60% do so for the LM1'. In all three scenarios, 100% of the events pass the $\not{E}_T$ cut so that we are only losing 20% to 40% of them by employing the m_{eff} cut. This is because the direct LSP decay modes of the scalar neutrinos (both the left handed and right handed one) are either not available or suppressed for the LM1', so that the $0\ell + \not{E}_T$ signal would emerge from indirect decay channels through $\widetilde{\chi}_2^0$ or $\widetilde{\chi}_4^0$ decays, with smaller branching ratio combinations. This can be understood from details provided earlier. The distributions for the secluded $U(1)'$ model dominate the ones for the MSSM since basically the total production cross section in the secluded $U(1)'$ model is much bigger.

The background distributions for the D-Y and ZZ processes are also included in the $\not{E}_T$ and E_T^{sum} graphs. The rate of success for the D-Y events passing both of the cuts are only about eight in 10^6. To give an idea how effective the m_{eff} cut is, the success rate of events was about a bit more than 3% before implementing the m_{eff} cut. The situation is even more drastic for the ZZ case. While the almost 100% of them passed the $\not{E}_T$ cut, this number goes down to 0.3% with the m_{eff} cut.

We included the $\hat{s}_{\text{min}}^{1/2}(0)$ graphs in the second row of Fig. 3 to estimate the mass scale of the parent particles, i.e., the left handed and right handed scalar neutrinos. The graph on the bottom right panel is nothing but the zoom-in version of the one left handed side for the secluded $U(1)'$ model. We cannot say anything about the MSSM case since the sum of the parent particle masses are varying in the $300\,\text{GeV}$ to $600\,\text{GeV}$ range, so that the $\hat{s}_{\text{min}}^{1/2}(0)$ peak is washed out due to the m_{eff} cut at $750\,\text{GeV}$. Indeed, for the secluded model we should expect two different peaks, one for the production of the left handed scalar neutrinos and the other one for the right handed ones. The peak for the left-handed sneutrinos which are much lighter are also washed out. We will see the picture clearer for the $4\ell + \not{E}_T$ signal.

In the right panel, we also indicated the positions of the peaks, which are correlated to the masses of the right handed scalar neutrinos. Of course, in reality to determine the peak position by fitting the data, a better job is needed . We just want to prove a point here. The peak position is related to the mass of $\widetilde{\nu}_{\ell_R}$ (since we produce them in pair)

$$m_{\widetilde{\nu}_{\ell_R}} \approx \frac{1}{2} \left(\hat{s}_{\text{min}}^{1/2}(0) \right)_{\text{peak}} . \tag{21}$$

From the peak positions in the graph we can estimate the average right handed sneutrino masses $m_{\widetilde{\nu}_{\ell_R}} \sim (530, 565, 600)\,\text{GeV}$ for the (LM1', LM2', LM6'), respectively, while the real average values should read $(460, 563, 654)\,\text{GeV}$ from Table IV. One source of error is not

knowing the mass of the LSP (though we find out that this is not significant here since the LSP mass is rather light and around $100\,\text{GeV}$) and the other is lack of a real fitting to the data to pin down the location of the peaks. The estimated values are still fairly good. We should also note that the method works better for signals with more visible particles.
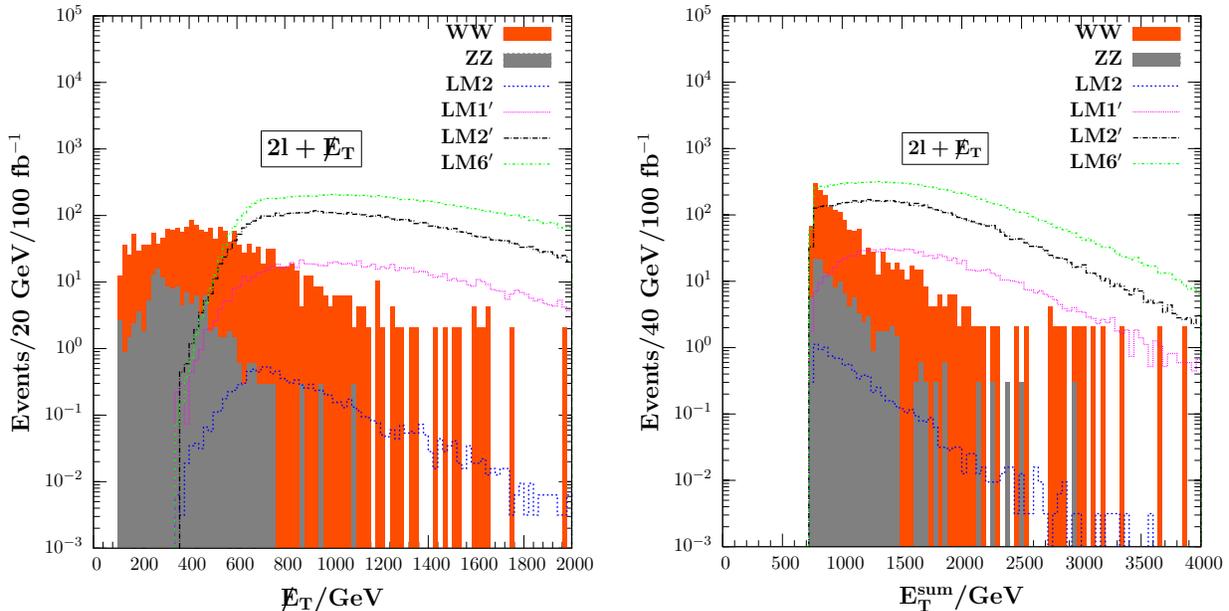
FIG. 4. *The $\not{E}_T$ and E_T^{sum} distributions of the $2\ell + \not{E}_T$ signal at $14\,\text{TeV}$ with integrated luminosity $\mathcal{L} = 100\ \text{fb}^{-1}$ for all three scenarios in the MSSM and secluded $U(1)'$ model.*

2. *The Dilepton Signal:* $2\ell + \not{E}_T$

We analyze the $2\ell + \not{E}_T$ signal in a similar fashion to the $0\ell + \not{E}_T$ one in the previous subsection. The results are shown in Fig. 4 and Fig. 5. The main background is from WW and ZZ. The D-Y does not contribute due to the transverse missing energy cut. After all the cuts, about 0.2% and 0.4% of the events pass for the WW and ZZ backgrounds, respectively. The rates were about 7% and 19%, respectively, before the m_{eff} cut. The situation for the $(\text{LM1}', \text{LM2}', \text{LM6}')$ scenarios after all the cuts signal is $(0.9\%, 50\%, 50\%)$ survival, but 100% in each cases before the m_{eff} cut. For the MSSM, only the LM2 gives $2\ell + \not{E}_T$ signal since, for the other two scenarios, the $\widetilde{\nu}_{\ell_L}\widetilde{\chi}_1^0$ are the only final staes. The number of events past the cuts for the LM2 decreases to 15% from 100% after inclusion of the m_{eff} cut.
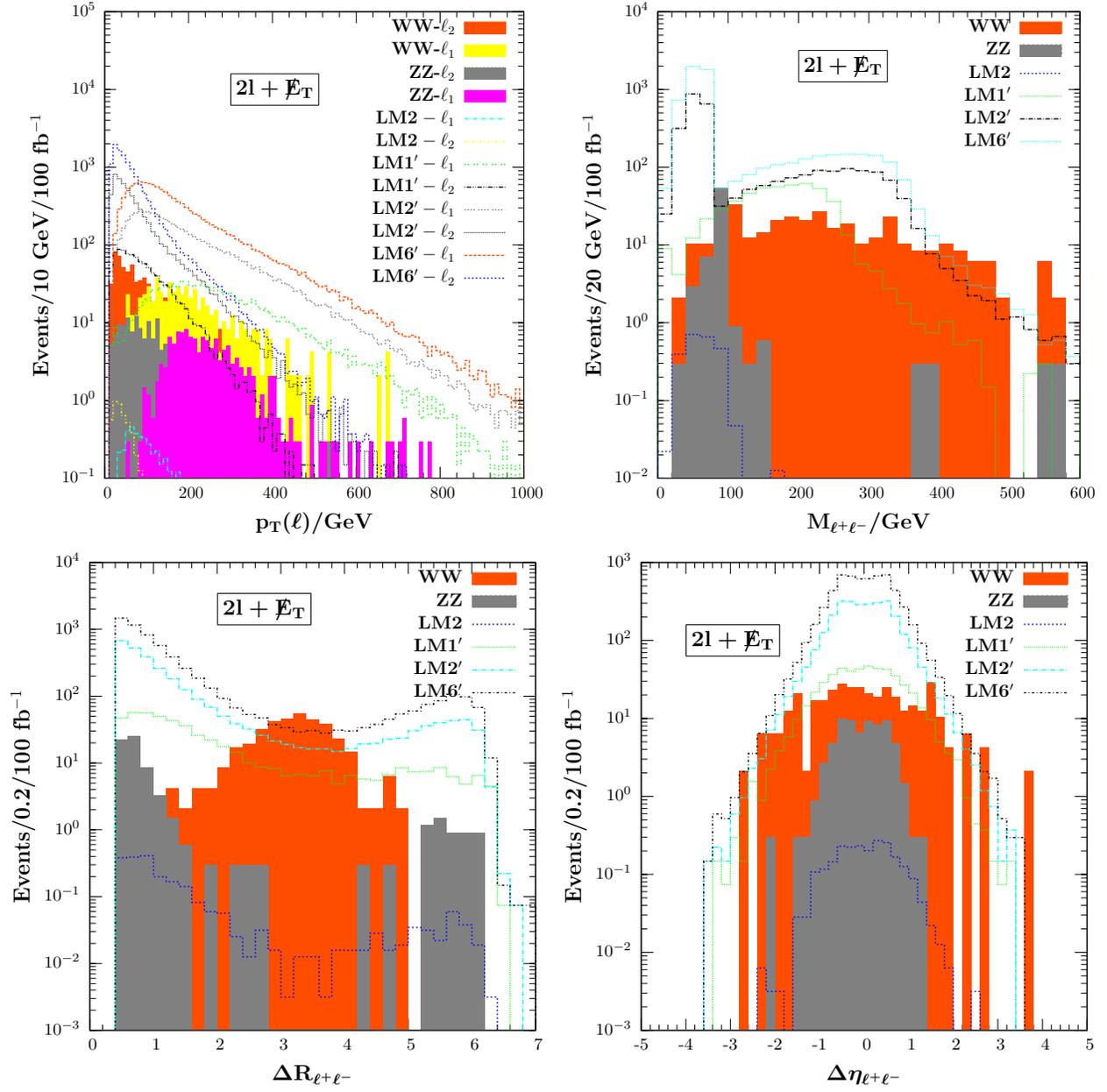
FIG. 5. *The* $p_T(\ell), M_{\ell^+\ell^-}, \Delta R_{\ell^+\ell^-}$ *and* $\Delta\eta_{\ell^+\ell^-}$ *distributions of the* $2\ell+\not{E}_T$ *signal at* $14\,\mathrm{TeV}$ *with integrated luminosity* $\mathcal{L} = 100\;\mathrm{fb}^{-1}$ *for all three scenarios in both MSSM and secluded* $U(1)'$ *model. Here,* ℓ_1 *represents the hardest lepton.*

We depicted the p_T spectra of both leptons ordered with respect to their hardness in Fig. 5. As expected the MSSM leptons are softer, and the distribution for ones from the LM2′ and LM6′ are very similar. The LM1′ scenario is somewhere in between. In the invariant mass of the leptons, the LM2′ and LM6′ curves peak at around 60 GeV and from the mass spectra in Table IV, the mass difference $m_{\widetilde{\chi}_2^0} - m_{\widetilde{\chi}_1^0}$ is between 75 GeV to 80 GeV.

The $2\ell + \not{E}_T$ signal mainly goes through $\widetilde{\chi}^0_2$. For the LM1$'$ the mass difference is $3\,\mathrm{GeV}$ and not visible. The ZZ peaks at around Z boson mass as expected.

In Fig. 5, we also include the $\Delta R_{\ell^+\ell^-}$ and $\Delta\eta_{\ell^+\ell^-}$ distributions. It is seen that for both the MSSM and the secluded $U(1)'$ model more leptons emerge with smaller separation, unlike the WW case the peak is at the point where the others have minimum. The background can be reduced further by adjusting the M_{eff} cut value. The leptons peak when they have the same pseudorapidity.

3. The Tetralepton Signal: $4\ell + \not{E}_T$

As we mentioned earlier, the $4\ell + \not{E}_T$ signal is practically background-free. The ZZ background disappears after the $\not{E}_T$ cut. Taking into account having relatively few $4\ell + \not{E}_T$ events, we relaxed the p_T and ΔR cut values. It is also true that MSSM scenarios LM1, LM2 and LM6 do not yield a $4\ell + \not{E}_T$ type of signal. For the LM1$'$, only 2% of the events pass the cuts and among them 1% of these are $2e2\mu$, while the rest of the events are shared between $4e$ and 4μ. The situation is different for the LM2$'$ and LM6$'$. The events which pass the cuts are around 68% for both cases and again half of them are the $2e2\mu$ type and the rest is shared equally between $4e$ and 4μ. In fact, there are more $4\ell + \not{E}_T$ events in the LM1$'$ scenario as compared to the other two scenarios (about 7.5% of $N_{\mathrm{tot}} = 4 \times 10^6$ for LM1$'$ but only 0.1% and 0.4% for LM2$'$ and LM6$'$, respectively). The reason is that the signal goes through $\widetilde{\chi}^0_2$ which is the dominant mode for the LM1$'$ but not for the LM2$'$ or LM6$'$. However, the cuts reduce the LM1$'$ events very significantly. Again the reason is the fact that $\widetilde{\chi}^0_2$ and $\widetilde{\chi}^0_1$ are almost degenerate for LM1$'$, which leads to very soft leptons.

In Fig. 6, $\not{E}_T$, E_T^{sum}, and $\hat{s}_{\mathrm{min}}^{1/2}(0)$ distributions of the $4\ell + \not{E}_T$ signal at $14\,\mathrm{TeV}$ with integrated luminosity $\mathcal{L} = 100$ fb^{-1} are shown for the three scenarios in the secluded $U(1)'$ model. As promised, we include a $\hat{s}_{\mathrm{min}}^{1/2}(0)$ graph with the peak correlated with the $\widetilde{\nu}_{\ell_L}\widetilde{\nu}^*_{\ell_L}$ production as well as the $\widetilde{\nu}_{\ell_R}\widetilde{\nu}^*_{\ell_R}$ production (no m_{eff} cut). We can roughly tell the positions of the peak without doing a serious fitting. For the LM1$'$, the first peak is around $250\,\mathrm{GeV}$ and the second one is around $950\,\mathrm{GeV}$. For the LM2$'$, they are at $(470\,\mathrm{GeV}, 1070\,\mathrm{GeV})$ for the first and the second peaks, respectively. For the LM6$'$, the peak positions are close to the LM2$'$ case, i.e., they are at $(490\,\mathrm{GeV}, 1110\,\mathrm{GeV})$. Then we can estimate the masses for LM1$'$/LM2$'$/LM6$'$
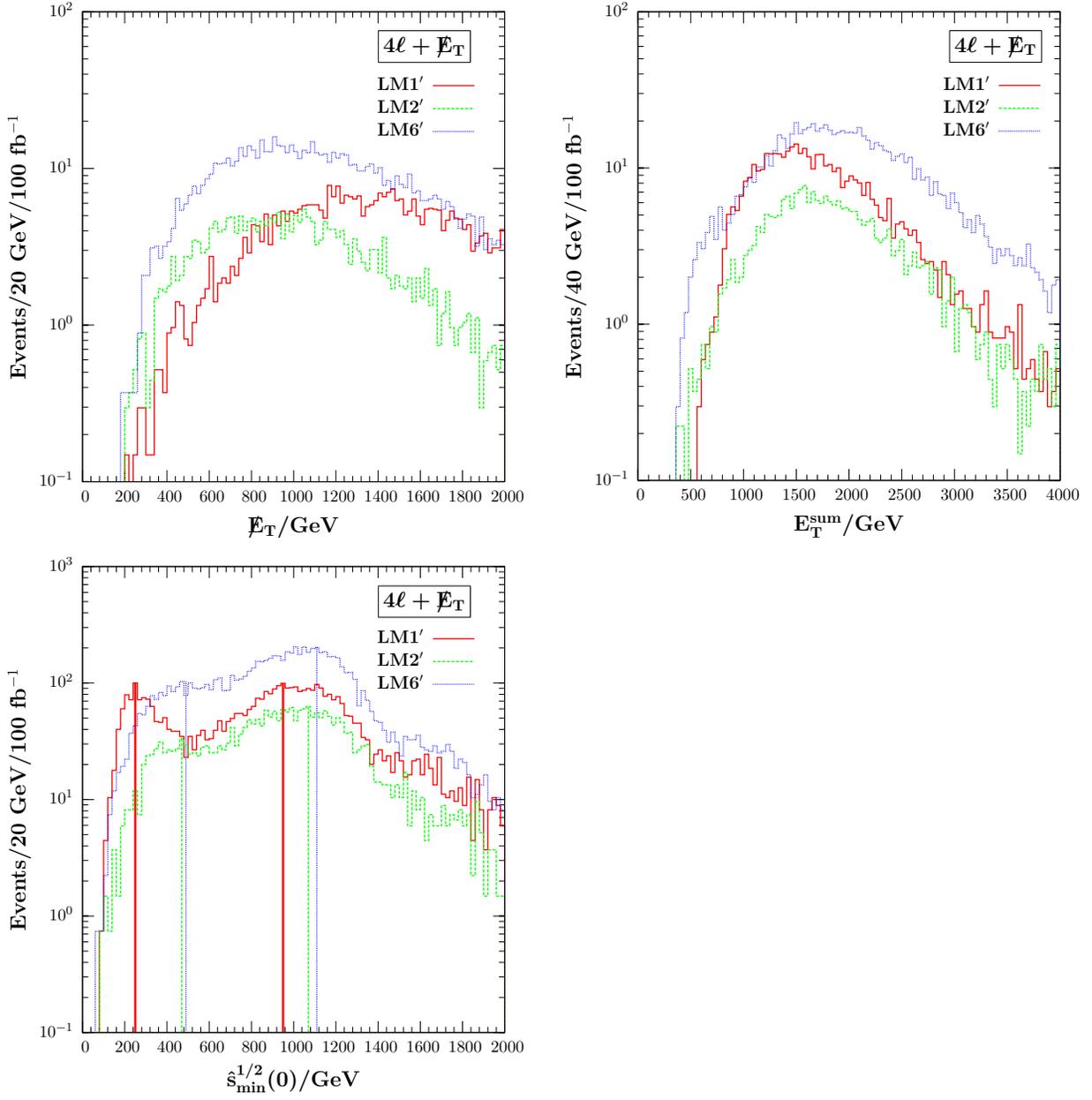
FIG. 6. The $\not{E}_T$, E_T^{sum} and $\hat{s}_{\min}^{1/2}(0)$ distributions of the tetralepton ($4\ell + \not{E}_T$) signal at 14 TeV with integrated luminosity $\mathcal{L} = 100$ fb^{-1}, for all three scenarios in the secluded $U(1)'$ model.

- $\left(m_{\widetilde{\nu}_{\ell_L}}, m_{\widetilde{\nu}_{\ell_R}} \right)_{\text{est.}} \approx (125\,\text{GeV}, 475\,\text{GeV}) \ / \ (235\,\text{GeV}, 535\,\text{GeV}) \ / \ (245\,\text{GeV}, 555\,\text{GeV})$

while the theoretical average values obtained, including three flavors

- $\left(m_{\widetilde{\nu}_{\ell_L}}, m_{\widetilde{\nu}_{\ell_R}} \right)_{\text{theo.}} \approx (132\,\text{GeV}, 460\,\text{GeV}) \ / \ (230\,\text{GeV}, 563\,\text{GeV}) \ / \ (258\,\text{GeV}, 654\,\text{GeV})$

We suspect that the deviations are mainly responsible for not determining the peak position after fitting the data to a curve. Also, simple averaging is not quite right. One should

25
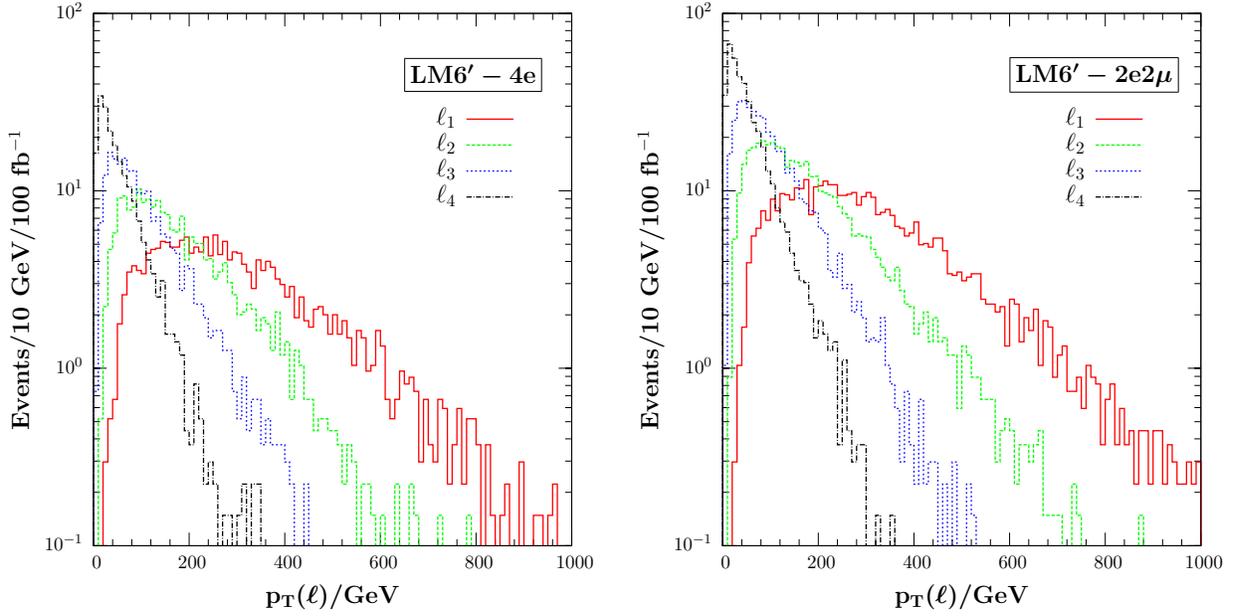
FIG. 7. *The p_T distribution of the $4e+$ $\not{E}_T$ and $2e2\mu+$ $\not{E}_T$ signals at 14 TeV with integrated luminosity $\mathcal{L} = 100$ fb^{-1} for all three scenarios in the secluded $U(1)'$ model. The $4\mu+$ $\not{E}_T$ case is similar. Also the hardness of the leptons are in decreasing order.*

include a relative weight based on the relative contributions from different flavor channels.

The p_T distributions of the $4e+$ $\not{E}_T$ and $2e2\mu+$ $\not{E}_T$ for LM6$'$ are given in Fig. 7. The 4μ case is very similar to $4e$. The leptons seem slightly more energetic for the $2e2\mu$ case than in the other cases. LM1$'$ and LM2$'$ have less energetic leptons and we do not include them here. Fig. 8 displays two-lepton invariant mass distributions for various possibilities. As expected only Opposite Sign Same Flavor (OSSF) distributions have peaks at the expected locations since both leptons originate from the same parent unlike the other cases, Same Sign Same Flavor (SSSF), Same Sign Opposite Flavor (SSOF) or Opposite Sign Opposite Flavor (OSOF). The next figure, Fig. 9, has four-lepton invariant mass distributions for $4e$ and $2e2\mu$ cases. The last two figures, Fig. 10 and Fig. 11, are devoted to the $\Delta R_{\text{SB(OB)}}$ and $\Delta\eta_{\text{SB(OB)}}$ distributions of the $4\ell+$ $\not{E}_T$ and $2e2\mu+$ $\not{E}_T$ signals. The subscript 'SB(OB)' stands for the Same Branch (Opposite Branch) and indicates where the leptons are coming from. We see that the distributions are very similar for 4ℓ and $2e2\mu$. If we compare ΔR_{SB} and ΔR_{OB}, the former peaks at small ΔR while the latter peaks larger distances. For the pseudorapidity, even though the shape of the distributions changes, they both peak when
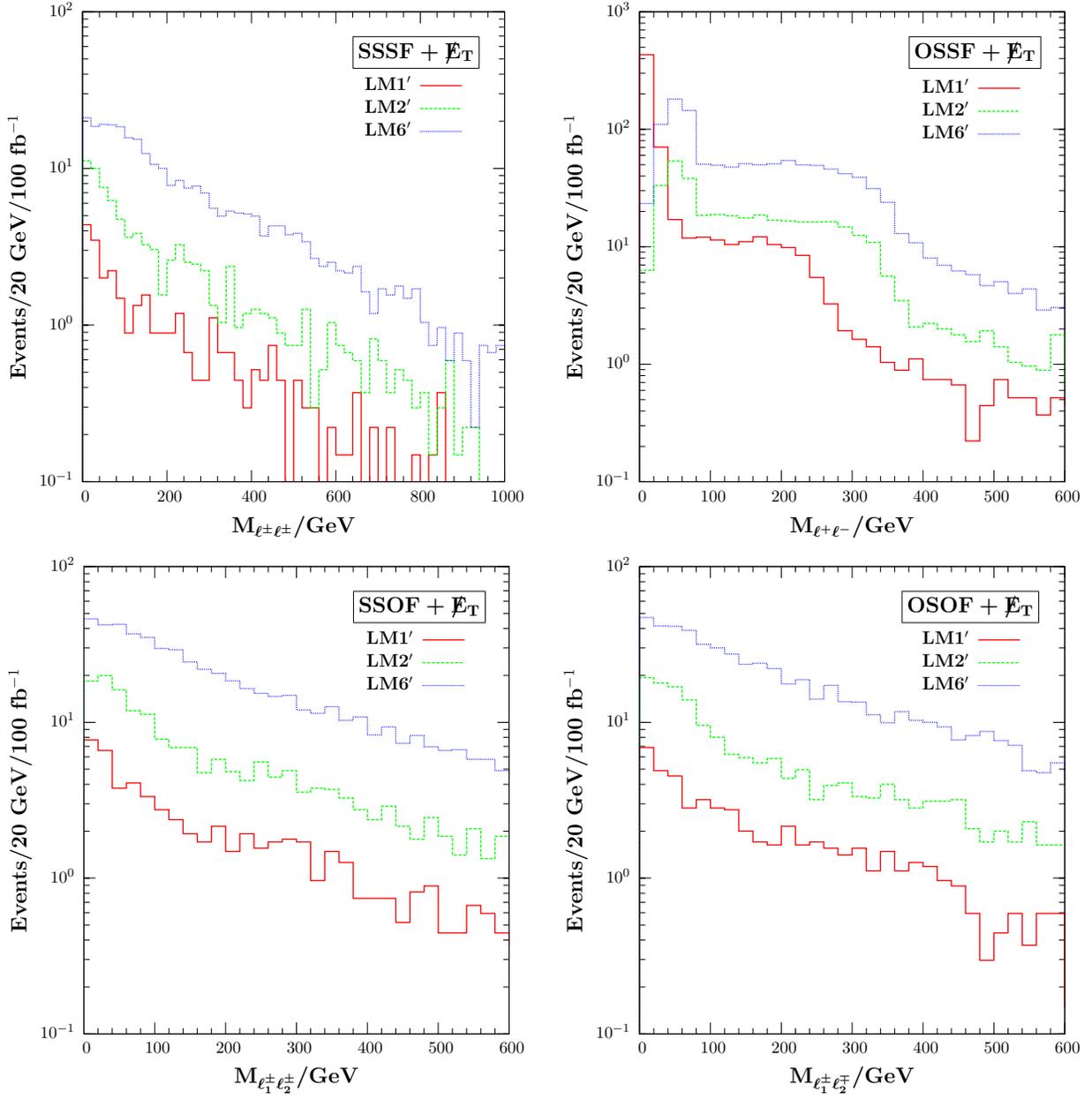
FIG. 8. *Various invariant mass distributions of the $4\ell + \not{E}_T$ signal at* $14\,\mathrm{TeV}$ *with integrated luminosity* $\mathcal{L} = 100$ fb^{-1} *for all three scenarios in the secluded* $U(1)'$ *model.*

the leptons have the same pseudorapidity.

IV. CONCLUSION

We presented a thorough and complete analysis of the scalar neutrino production and decays in a $U(1)'$ model endowed with a secluded sector. This model has several attractive
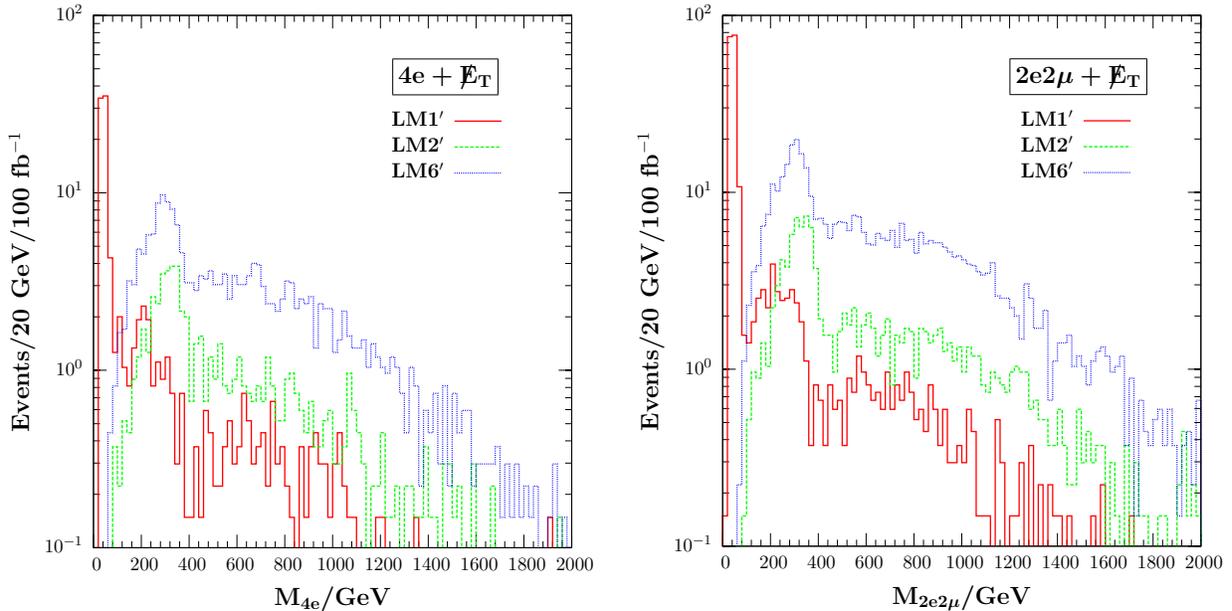
FIG. 9. *Four lepton invariant mass distributions of $4\ell+\not{E}_T, \ell = e, \mu$ and $2e2\mu+\not{E}_T$ signals at 14 TeV with integrated luminosity $\mathcal{L} = 100$ fb^{-1} for all three scenarios in the secluded $U(1)'$ model.*

features as compared to the MSSM. First, it extends the gauge symmetry to include an extra neutral gauge boson, allowing for the presence of right handed neutrinos. Neutrinos are Dirac particles in this model, and masses are provided through an effective neutrino Yukawa coupling which is naturally suppressed by the $U(1)'$ invariance. This model generates the μ term dynamically, through the VEV of a singlet scalar field. The secluded sector consists of three chiral superfields in addition to $\widehat{S}$, and generates correct Z'/Z mass hierarchy without affecting the μ parameter. Previous studies have provided extensive phenomenological analyses of this model, and notably, have provided a novel way to explain the excess positron flux in cosmic rays.

The model has three right-handed scalar neutrinos, in addition to the three left-handed states from the SM/MSSM spectrum. Cross sections are considerably enhanced compared to the ones estimated in MSSM, even though for most of the parameter space studied, the signal is dominated by production of left handed sneutrinos, predicted to be lighter. To perform a through analysis, we concentrate on three MSSM benchmark parameter points, denoted by LM1, LM2 and LM6 and define correspondingly three $U(1)'$ parameter points, denoted by LM1', LM2', LM6', specified in such that the common parameters with MSSM are identical. At this point, it is convenient to give a couple of remarks on the scenarios adopted here. As
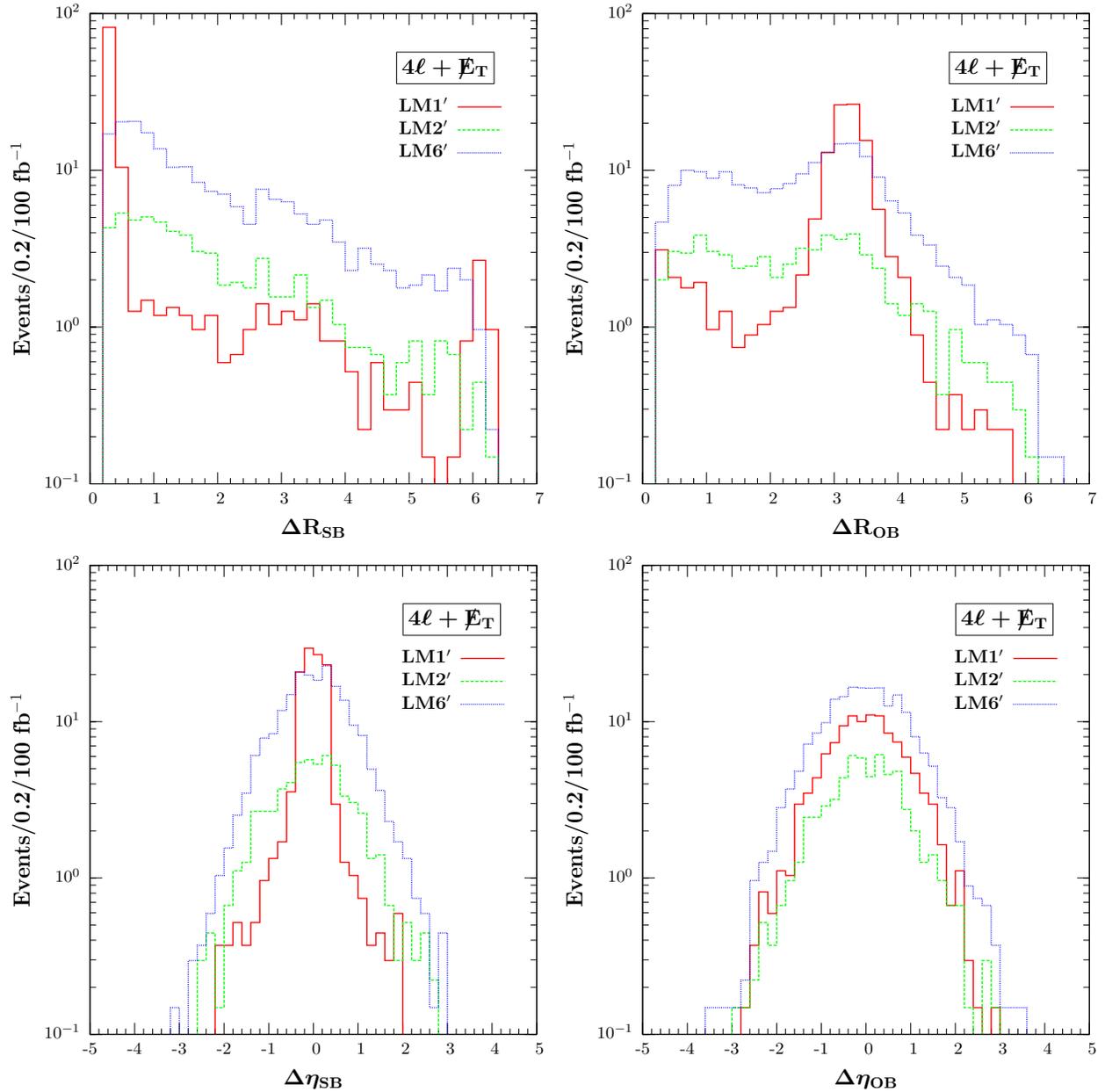
FIG. 10. *The $\Delta R_{\ell^+\ell^-}$ and $\Delta\eta_{\ell^+\ell^-}$ distributions of the $4\ell + \not{E}_T$ signal at 14 TeV with integrated luminosity $\mathcal{L} = 100$ fb^{-1} for all three scenarios in the secluded $U(1)'$ model. Here and in what follows, 'SB' is short-hand for 'Same Branch' and 'OB' for 'Opposite Branch'.*

we mentioned earlier, a $U(1)'$ model with one singlet and right handed sneutrinos [8] can explain the excess positron flux observed by various satellite experiments. However, this requires a rather special mass spectrum. Indeed, it turns out that the LSP must one of the right handed scalar neutrinos with a mass around 100 GeV, and the next-to-LSP must also be a right handed scalar neutrino weighing at the TeV scale. All the other SUSY particles

29
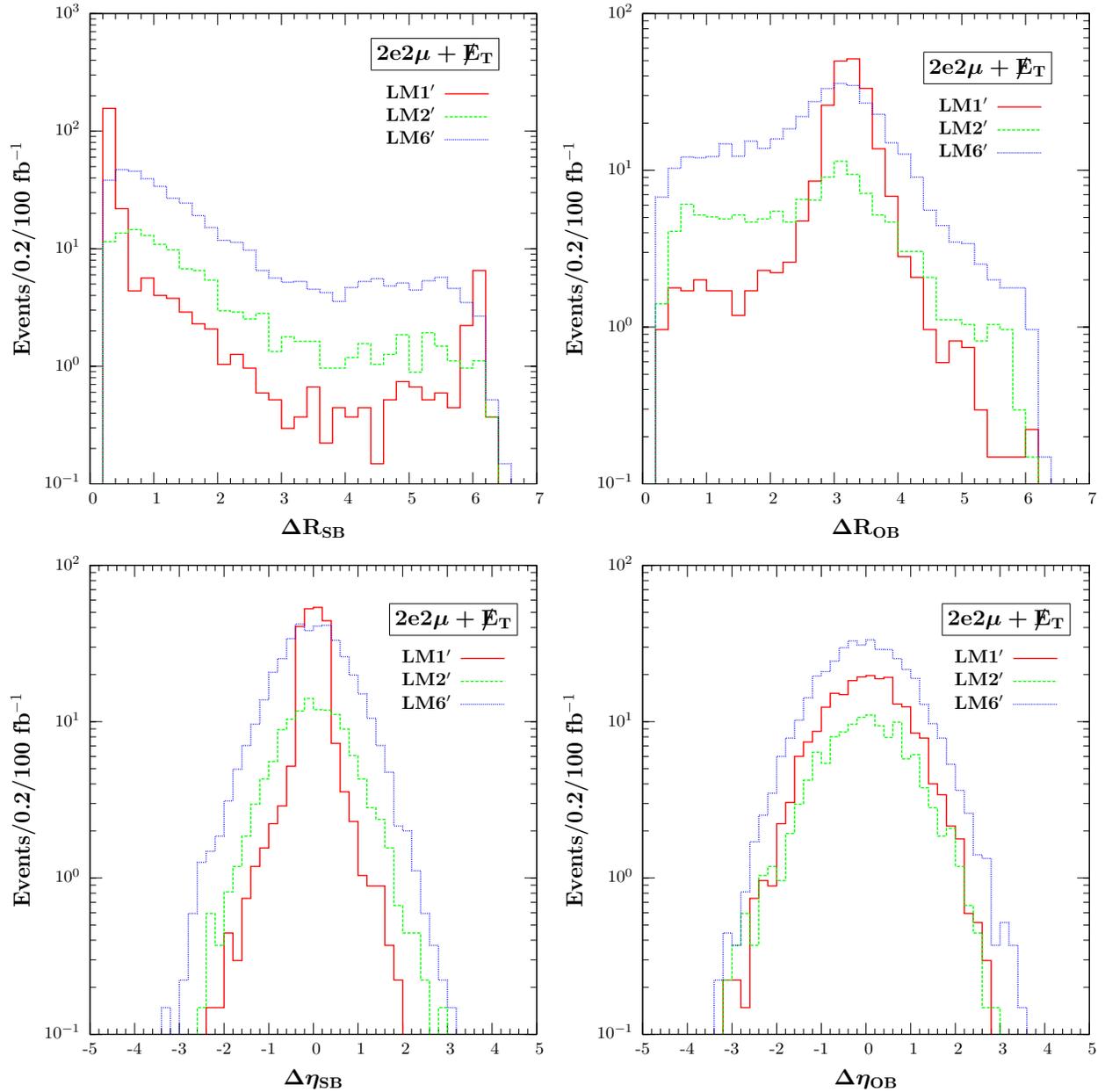
FIG. 11. *The $\Delta R_{\ell^+\ell^-}$ and $\Delta\eta_{\ell^+\ell^-}$ distributions of the $2e2\mu + \not{E}_T$ signal at $14\,\mathrm{TeV}$ with integrated luminosity $\mathcal{L} = 100\ \mathrm{fb}^{-1}$ for all three scenarios in the secluded $U(1)'$ model.*

have to be heavier. One might ask why we did not consider such a scenario here. There are a couple of reasons. First of all, excess positron flux observation doesn't need to have an explanation coming from particle physics, only. Secondly, the signal for such a scenario would be mainly just missing transverse energy since all the SUSY particles other than the LSP are above the TeV scale so that the cross section for left-handed sneutrino production would be much smaller. Practically, missing energy signal with no visible particle is not

useful experimentally. Finally, in this work, we focused on only low-scale SUSY scenarios which would be discovered with the early LHC data at 14 TeV.

After producing and decaying the sneutrinos, we identify three final-state signals: $0\ell + \not{E}_T$, $2\ell + \not{E}_T$ and $4\ell + \not{E}_T$ and proceed to analyze them at LHC, for 14 TeV center-of-mass energy and with integrated luminosity $\mathcal{L} = 100$ fb^{-1}. We compare these signals with the $0\ell + \not{E}_T$ and $2\ell + \not{E}_T$ signals in MSSM, and discuss the SM background (coming from Drell Yan, ZZ and WW production) for each. While $0\ell + \not{E}_T$ is the strongest, it has to compete with MSSM and suffers from considerable background suppression, while the $4\ell + \not{E}_T$ signal has no MSSM equivalent, is practically background free, but has few events.

We analyze the signals and suggest cuts to distinguish it from the background. In particular $E_T^{\text{sum}} \equiv m_{\text{eff}}$, the scalar sum of the lepton transverse momenta and the missing energy is found to be high for the signal, thus a cut on m_{eff} will likely reduce the background. Additionally a new parameter $\hat{s}_{\text{min}}^{1/2}$ is found to be useful for estimating the mass of parent particles in hard scattering. (The peak in $\hat{s}_{\text{min}}^{1/2}$ gives the mass threshold of left and right handed sneutrinos in the decay process). Using these considerations, we can estimate the production cross section, the products of decay and estimate the sneutrino masses. The MSSM production differs both in the number of events expected, cross section, E_T^{sum}, $\hat{s}_{\text{min}}^{1/2}$, in the $0\ell + \not{E}_T$ case; and additionally in the p_T spectra of leptons (for $2\ell + \not{E}_T$ case). The $4\ell + \not{E}_T$ case has no MSSM equivalent and little, if any, background, so the $U(1)'$ is clear there; however the number of events, especially after passing detector cuts, is small.

In conclusion, our extensive analysis shows significant enhancement of $U(1)'$ signal over the MSSM signal in sneutrino production and decays, and indicates how the two models can be distinguished from each other and the background. This provides a distinct collider signal for the secluded $U(1)'$ model at the LHC.

V. ACKNOWLEDGMENTS

Appendix A: The Lagrangian

In this Appendix, we present the complete Lagrangian of the $U(1)'$ model and highlight the differences between this and the MSSM Lagrangian. Although parts of this formulation have appeared elsewhere [7, 15, 25], we include the complete model information for consistency, and to help future studies. The total Lagrangian incorporates kinetic terms and various interaction terms among the fields. We discuss below the distinct pieces separately.

The kinetic terms of the Lagrangian are given by

$$\mathcal{L}_{U(1)'}^{Kinetic} = \mathcal{L}_{MSSM}^{Kinetic} - \frac{1}{4} Z'^{\mu\nu} Z'_{\mu\nu} + (\mathcal{D}_\mu S)^\dagger (\mathcal{D}^\mu S) + \tilde{Z}'^\dagger i \sigma^\mu \partial_\mu \tilde{Z}' + \tilde{S}^\dagger i \sigma^\mu \mathcal{D}_\mu \tilde{S}$$
$$+ (\mathcal{D}_\mu S_j)^\dagger (\mathcal{D}^\mu S_j) + \tilde{S}_j^\dagger i \sigma^\mu \mathcal{D}_\mu \tilde{S}_j + (\mathcal{D}_\mu \tilde{N})^\dagger (\mathcal{D}^\mu \tilde{N}) \qquad (A1)$$

where $j = 1, 2, 3$. The interactions of the gauge fields with the rest (fermions, sfermions, gauginos, Higgs and Higgsino fields) are contained in the piece

$$\mathcal{L}_{U(1)'}^{gauge} = \mathcal{L}_{MSSM}^{gauge} \left(g_Y \frac{Y_X}{2} B_\mu \to g_Y \frac{Y_X}{2} B_\mu + g_{Y'} Q'_X Z'_\mu \right) , \qquad (A2)$$

where X runs over the fields charged under $U(1)'$. In (A1), $Z'^{\mu\nu}$ is the field strength tensor of Z'_μ, and $\mathcal{D}_\mu S_j = (\partial_\mu + i g_{Y'} Q'_{S_j} Z'_\mu) S_j$ for $j = 1, 2, 3$.

The part of the $U(1)'$ Lagrangian spanned by the F–terms is given by

$$\mathcal{L}_{U(1)'}^{F-term} = - \sum_i \left| \frac{\partial W}{\partial \phi_i} \right|^2 = \mathcal{L}_{MSSM}^{F-term}(\mu \to h_s S) - h_s^2 |H_u \cdot H_d|^2$$
$$- \left(h_u \tilde{Q}^* \tilde{U}^* + h_s^* S^* H_d^* \right) \frac{h_\nu}{M_R} S_1 \tilde{L} \tilde{N}$$
$$- \frac{h_\nu}{M_R} S_1^* \tilde{L}^* \tilde{N}^* \left(h_u \tilde{Q} \tilde{U} + h_s S H_d + \frac{h_\nu}{M_R} S_1 \tilde{L} \tilde{N} \right)$$
$$- \left(h_e H_d^* \tilde{E}^* \right) \frac{h_\nu}{M_R} S_1 H_u \tilde{N}$$
$$- \frac{h_\nu}{M_R} S_1^* H_u^* \tilde{N}^* \left(h_e H_d \tilde{E} + \frac{h_\nu}{M_R} S_1 H_u \tilde{N} \right)$$
$$- \frac{h_\nu^2}{M_R^2} S_1^2 |\tilde{L} \cdot H_u|^2$$

$$-\frac{h_\nu^2}{M_R^2}|\tilde{L}\cdot H_u|^2\tilde{N}^2 - \bar{h}_s^2 S_2^2 S_3^2$$

$$-\frac{h_\nu}{M_R}\tilde{L}^*\cdot H_u^*\tilde{N}^*\bar{h}_s S_2 S_3 - \bar{h}_s S_2^* S_3^*\frac{h_\nu}{M_R}\tilde{L}\cdot H_u\tilde{N}$$

$$-\bar{h}_s^2 S_1^2 S_3^2 - \bar{h}_s^2 S_1^2 S_2^2 \tag{A3}$$

where ϕ_i is the scalar component of the i–the chiral superfield in the superpotential.

The D–term contributions to the Lagrangian are given by

$$\mathcal{L}_{U(1)'}^{D-term} = -\frac{1}{2}\sum_a D^a D^a = \mathcal{L}_{MSSM}^{D-term}$$

$$-\frac{g_{Y'}^2}{2}\Big(Q_Q'\tilde{Q}^*\tilde{Q} + Q_U'\tilde{U}^*\tilde{U} + Q_D'\tilde{D}^*\tilde{D} + Q_L'\tilde{L}^*\tilde{L} + Q_E'\tilde{E}^*\tilde{E}$$

$$+ Q_{H_d}'H_d^*H_d + Q_{H_u}'H_u^*H_u + Q_N'\tilde{N}^*\tilde{N} + Q_S'S^*S + Q_{S_1}'S_1^*S_1$$

$$+ Q_{S_2}'S_2^*S_2 + Q_{S_3}'S_3^*S_3\Big)^2 \tag{A4}$$

The soft-breaking sector of the $U(1)'$ Lagrangian is

$$\mathcal{L}_{U(1)'}^{Soft} = \mathcal{L}_{MSSM}^{Soft}(\mu\to 0) - m_S^2 S^*S - m_{S_1}^2 S_1^*S_1 - m_{S_2}^2 S_2^*S_2 - m_{S_3}^2 S_3^*S_3 - m_N^2\tilde{N}^*\tilde{N}$$

$$- [h_s A_s S H_u\cdot H_d + \frac{h_\nu}{M_R}A_\nu S_1\tilde{L}\cdot H_u\tilde{N} + A_{\bar{h}_s}\bar{h}_s S_1 S_2 S_3 + h.c.]$$

$$+ \frac{1}{2}\Big(M_{\tilde{Z}'}\tilde{Z}'\tilde{Z}' + h.c.\Big)$$

$$+ (m_{SS_1}^2 SS_1 + m_{SS_2}^2 SS_2 + m_{S_1S_2}^2 S_1^*S_2 + h.c.) \tag{A5}$$

where $M_{\tilde{Z}'}$ is $U(1)'$ gaugino mass defined below in (C2), and A_s is the extra trilinear soft coupling.

Finally, the part of the Lagrangian describing the fermion-sfermion-ino interactions, as well as the Higgs-Higgsino-Higgsino interactions, is given by

$$\mathcal{L}_{U(1)'}^{ino-f-\phi} = \mathcal{L}_{MSSM}^{ino-f-\phi}(\mu\to 0) + i\sqrt{2}g_{Y'}[Q_Q'Q^\dagger\tilde{Z}'\tilde{Q} + Q_U'u_R^\dagger\tilde{Z}'\tilde{u}_R$$

$$+ Q_D'd_R^\dagger\tilde{Z}'\tilde{d}_R + Q_L'L^\dagger\tilde{Z}'\tilde{L} + Q_E'\ell_R^\dagger\tilde{Z}'\tilde{\ell}_R + Q_{H_d}'\tilde{H}_d^\dagger\tilde{Z}'H_d$$

$$+ Q_{H_u}'\tilde{H}_u^\dagger\tilde{Z}'H_u + Q_S'\tilde{S}^\dagger\tilde{Z}'S + Q_{S_j}'\tilde{S}_j^\dagger\tilde{Z}'S_j + Q_N'\nu_R^\dagger\tilde{Z}'\tilde{\nu}_R + h.c.]$$

$$+ [h_s S\tilde{H}_u\cdot\tilde{H}_d + h_s\tilde{S}H_u\cdot\tilde{H}_d + h_s\tilde{S}\tilde{H}_u\cdot H_d + h.c.]. \tag{A6}$$

All parts of the the $U(1)'$ model Lagrangian listed above are described in the current basis. Eventually, the fields must be transformed into the physical basis where each field obtains a definite mass. The neutral gauginos and Higgsinos form the neutralino sector whose physical states are expressed as in (C1), after diagonalizing the mass matrix (C2).

Unlike the neutralino sector, the structure of the chargino sector is essentially the same as in the MSSM with the replacement $\mu \to h_s v_s / \sqrt{2}$. A detailed analysis of the Higgs and chargino sectors of the $U(1)'$ model has been given in [7].

In the gauge boson sector, spontaneous breakdown of the product group $SU(2)_L \otimes U(1)_Y \otimes U(1)'$ via the Higgs VEVs

$$\langle H_u \rangle = \frac{1}{\sqrt{2}} \begin{pmatrix} 0 \\ v_u \end{pmatrix}, \quad \langle H_d \rangle = \frac{1}{\sqrt{2}} \begin{pmatrix} v_d \\ 0 \end{pmatrix}, \quad \langle S \rangle = \frac{v_s}{\sqrt{2}}, \quad \langle S_i \rangle = \frac{v_{s_i}}{\sqrt{2}} \tag{A7}$$

generates one massless state (the photon) and two massive states (the Z, Z' bosons) via orthonormal combinations of W_μ^3, B_μ' and B_μ gauge bosons. The W_μ^1 and W_μ^2 linearly combine to give $W_\mu^\pm$, as the only charged vector bosons in the model. In contrast to the MSSM, the Z boson is not a physical state by itself since it mixes with the Z' boson. This mass mixing arises from the fact that the Higgs doublets $H_{u,d}$ are charged under each factor of $SU(2)_L \otimes U(1)_Y \otimes U(1)'$, and the associated mass-squared matrix is given by [25, 26]

$$M_{Z-Z'}^2 = \begin{pmatrix} M_Z^2 & \Delta^2 \\ \Delta^2 & M_{Z'}^2 \end{pmatrix}, \tag{A8}$$

in the (Z_μ, Z_μ') basis. Its entries are

$$M_Z^2 = \frac{1}{4} G_Z^2 \left(v_u^2 + v_d^2 \right),$$

$$M_{Z'}^2 = g_{Y'}^2 \left(Q_{H_u}'^2 v_u^2 + Q_{H_d}'^2 v_d^2 + Q_S'^2 v_s^2 + \sum_{i=1}^{3} Q_{S_i}'^2 v_{s_i}^2 \right),$$

$$\Delta^2 = \frac{1}{2} G_Z g_{Y'} \left(Q_{H_u}' v_u^2 - Q_{H_d}' v_d^2 \right), \tag{A9}$$

where $G_Z^2 = g_2^2 + g_Y^2$. The physical neutral vector bosons, $Z_{1,2}$, are obtained by diagonalizing $M_{Z-Z'}^2$:

$$\begin{pmatrix} Z_1 \\ Z_2 \end{pmatrix} = \begin{pmatrix} \cos\theta_{Z-Z'} & \sin\theta_{Z-Z'} \\ -\sin\theta_{Z-Z'} & \cos\theta_{Z-Z'} \end{pmatrix} \begin{pmatrix} Z \\ Z' \end{pmatrix}, \tag{A10}$$

where

$$\theta_{Z-Z'} = -\frac{1}{2} \arctan \left(\frac{2\Delta^2}{M_{Z'}^2 - M_Z^2} \right), \tag{A11}$$

is their mass mixing angle, and

$$M_{Z_{1(2)}}^2 = \frac{1}{2} \left[M_{Z'}^2 + M_Z^2 - (+) \sqrt{(M_{Z'}^2 - M_Z^2)^2 + 4\Delta^4} \right], \tag{A12}$$

are their masses-squared . The collider searches at LEP and Tevatron plus various indirect observations require Z–Z' mixing angle $\theta_{Z-Z'}$ to be at most a few 10^{-3} with an unavoidable model dependence coming from the Z' couplings [26–31]. This bound requires either M_{Z_2} to be large enough (well in the TeV range) or Δ^2 to be sufficiently suppressed by the vacuum configuration, that is, $\tan^2 \beta \equiv v_u^2/v_d^2 \sim Q'_{H_d}/Q'_{H_u}$. Which of these options is realized depends on the $U(1)'$ charge assignments and the soft-breaking masses in the Higgs sector (see [7] for a variant for reducing the Z–Z' mixing).

Appendix B: The Scalar Fermions

Given rather tight FCNC bounds, we neglect all the inter-generational mixings, and consider only intra-generational left-right mixings, though these turn out to be totally negligible for the sfermions in the first and second generations. The 2×2 scalar fermion mixing matrix can be written as

$$
\mathcal{M}_{\tilde{f}^a}^2 = \begin{pmatrix} \mathcal{M}_{\tilde{f}_{LL}^a}^2 & \mathcal{M}_{\tilde{f}_{LR}^{a,b}}^2 \\[2ex] \mathcal{M}_{\tilde{f}_{LR}^{a,b}}^{2\dagger} & \mathcal{M}_{\tilde{f}_{RR}^a}^2 \end{pmatrix} , \qquad a \neq b = u, d \, , \tag{B1}
$$

where

$$
\begin{aligned}
\mathcal{M}_{\tilde{f}_{LL}^\alpha}^2 &= \tilde{M}_{\tilde{f}_L}^2 + \frac{1}{2} h_{f^\alpha}^2 v_\alpha^2 \kappa_s^2 + \frac{1}{4}\left[g_Y^2 Y_{f_L^\alpha} - (+)\frac{g^2}{2} \right] (v_u^2 - v_d^2) \\
&\quad + \frac{1}{2} g_{Y'}^2 Q'_{f_L^\alpha} (Q'_{H_u} v_u^2 + Q'_{H_d} v_d^2 + Q'_S v_s^2 \rho_s)
\end{aligned} \tag{B2}
$$

$$
\begin{aligned}
\mathcal{M}_{\tilde{f}_{RR}^\alpha}^2 &= \tilde{M}_{\tilde{f}_R}^2 + \frac{1}{2} h_{f^\alpha}^2 v_\alpha^2 \kappa_s^2 + \frac{1}{4}\left[g_Y^2 Y_{f_R^\alpha} \right] (v_u^2 - v_d^2) \\
&\quad + \frac{1}{2} g_{Y'}^2 Q'_{f_R^\alpha} (Q'_{H_u} v_u^2 + Q'_{H_d} v_d^2 + Q'_S v_s^2 \rho_s)
\end{aligned} \tag{B3}
$$

$$
\mathcal{M}_{\tilde{f}_{LR}^{\alpha,\beta}}^2 = (\mathcal{M}_{\tilde{f}_{RL}^{\alpha,\beta}}^2)^* = \frac{h_{f^\alpha} \kappa_s}{2\sqrt{2}} (\pm 2 A_{f^\alpha}^* v_\alpha + \sqrt{2} h_s v_\beta v_s + 2\sqrt{2}\xi_s) \tag{B4}
$$

where $\kappa_s = \frac{v_{s_1}}{\sqrt{2} M_R}$ and $\xi_s = \frac{\bar{h}_s v_{s_2} v_{s_3} v_u}{2 v_{s_1}}$ for sneutrinos and $\kappa_s = 1$ and $\xi_s = 0$ for the others. Here $\tilde{M}_{\tilde{f}_{L,R}}^2$ are the soft mass-squared of the sfermions, v_{u,d,s,s_1,s_2,s_3} are the VEVs of the Higgs fields, $Y_{f^a} (T_{3L})$ is the $U(1)_Y$ $(SU(2)_L)$ quantum number, Q'_{f^a} is the $U(1)'$ charge, and A_{f^a} are the trilinear couplings. The mixing matrix can be diagonalized, in general, by a unitary matrix Γ^f such that $\Gamma^{f^a\dagger} \cdot \mathcal{M}_{\tilde{f}^a}^2 \cdot \Gamma^{f^a} \equiv \mathrm{Diag}(M_{\tilde{f}_1^a}^2, M_{\tilde{f}_2^a}^2)$.[‡] The rotation matrix Γ^{f^a} can be

---

[‡] We note that unlike mixings in other sectors, Γ^{f^a} is defined differently, that is, $(\tilde{f}_{L,R}^a)_i = \Gamma_{ij}^{f^a} \tilde{f}_j^a$, where $\tilde{f}_j^a$ represent the mass eigenstates.

written for quarks and charged leptons in the 2×2 $\{\widetilde{f}_L^a, \widetilde{f}_R^a\}$ basis as

$$\Gamma^{f^a} = \begin{pmatrix} \cos\theta_{\widetilde{f}^a} & -\sin\theta_{\widetilde{f}^a} \\ \sin\theta_{\widetilde{f}^a} & \cos\theta_{\widetilde{f}^a} \end{pmatrix},$$ (B5)

where $\theta_{\widetilde{f}^a} = \frac{1}{2}\arctan 2(-2\mathcal{M}^2_{\widetilde{f}^a_{LR}}, \mathcal{M}^2_{\widetilde{f}^a_{RR}} - \mathcal{M}^2_{\widetilde{f}^a_{LL}})$ and $\arctan 2(y,x)$ is defined as

$$\arctan 2(y,x) = \begin{cases} \phi \, \mathrm{sign}(y), & x > 0 \\ \frac{\pi}{2} \, \mathrm{sign}(y), & x = 0 \\ (\pi - \phi) \, \mathrm{sign}(y), & x < 0 \end{cases}$$ (B6)

with y being non-zero, and ϕ taken in the first quadrant such that $\tan\phi = |y/x|$.

For the sfermions in the first and second generations, the left-right mixings are exceedingly small as they are proportional to the corresponding fermion mass. Therefore, the sfermion mass matrix (B2) is automatically diagonal. However, one has to remember that the sfermion masses, for fixed values of $m_{\widetilde{f}^2_{L,R}}$, are different in the MSSM than in the $U(1)'$ models due to the additional D-term contribution in the latter.

Appendix C: Gauge and Higgs Fermions

Although the $U(1)'$ model possesses no new charged Higgsinos and gauginos it possesses five new fermion fields in the neutral sector: the $U(1)'$ gauge fermion $\widetilde{Z}'$ and four singlinos $\widetilde{S}, \widetilde{S}_1, \widetilde{S}_2, \widetilde{S}_3$. In total, there are 9 neutralino states $\widetilde{\chi}_i^0$ $(i = 1, \ldots, 9)$ [7]:

$$\widetilde{\chi}_i^0 = \sum_a N_{ia}^0 \widetilde{G}_a \,,$$ (C1)

where the mixing matrix N_{ia}^0 connects the gauge-basis neutral fermion states $\widetilde{G}_a \in \{\widetilde{B}, \widetilde{W}^3, \widetilde{H}_d^0, \widetilde{H}_u^0, \widetilde{S}, \widetilde{Z}', \widetilde{S}_1, \widetilde{S}_2, \widetilde{S}_3\}$ to the physical neutralinos $\widetilde{\chi}_i^0$. The neutralino masses $M_{\widetilde{\chi}_i^0}$ and the mixing matrix N_{ia}^0 are determined via the diagonalization condition $N^0 \mathcal{M} N^{0\,T} = \mathrm{Diag}$ $\{M_{\widetilde{\chi}_1^0}, \ldots, M_{\widetilde{\chi}_9^0}\}$ for the neutral fermion mass matrix

$$
\begin{pmatrix}
M_{\tilde{Y}} & 0 & -M_{\tilde{Y}\tilde{H}_d} & M_{\tilde{Y}\tilde{H}_u} & 0 & M_{\tilde{Y}\tilde{Z}'} & 0 & 0 & 0 \\[4pt]
0 & M_{\tilde{W}} & M_{\tilde{W}\tilde{H}_d} & -M_{\tilde{W}\tilde{H}_u} & 0 & 0 & 0 & 0 & 0 \\[4pt]
-M_{\tilde{Y}\tilde{H}_d} & M_{\tilde{W}\tilde{H}_d} & 0 & -\mu & -\mu_{H_u} & \mu'_{H_d} & 0 & 0 & 0 \\[4pt]
M_{\tilde{Y}\tilde{H}_u} & -M_{\tilde{W}\tilde{H}_d} & -\mu & 0 & -\mu_{H_d} & \mu'_{H_u} & 0 & 0 & 0 \\[4pt]
0 & 0 & -\mu_{H_u} & -\mu_{H_d} & 0 & \mu'_S & 0 & 0 & 0 \\[4pt]
M_{\tilde{Y}\tilde{Z}'} & 0 & \mu'_{H_d} & \mu'_{H_u} & \mu'_S & M_{\tilde{Z}'} & \mu'_{S_1} & \mu'_{S_2} & \mu'_{S_3} \\[4pt]
0 & 0 & 0 & 0 & 0 & \mu'_{S_1} & 0 & -\frac{\bar{h}_s v_{s_3}}{\sqrt{2}} & -\frac{\bar{h}_s v_{s_2}}{\sqrt{2}} \\[4pt]
0 & 0 & 0 & 0 & 0 & \mu'_{S_2} & -\frac{\bar{h}_s v_{s_3}}{\sqrt{2}} & 0 & -\frac{\bar{h}_s v_{s_1}}{\sqrt{2}} \\[4pt]
0 & 0 & 0 & 0 & 0 & \mu'_{S_3} & -\frac{\bar{h}_s v_{s_2}}{\sqrt{2}} & -\frac{\bar{h}_s v_{s_1}}{\sqrt{2}} & 0
\end{pmatrix}
\tag{C2}
$$

where certain entries are generated by the soft-breaking sector while others follow from the $SU(3)_c \otimes SU(2)_L \otimes U(1)_Y \otimes U(1)'$ breaking. The $U(1)_Y$ gaugino mass $M_{\tilde{Y}}$, the $SU(2)_L$ gaugino mass $M_{\widetilde{W}}$, and the $U(1)'$ gaugino mass

$$
M_{\tilde{Z}'} = \frac{M_{\widetilde{Y}'}}{\cos^2 \chi} - 2\frac{\tan \chi}{\cos \chi} M_{\widetilde{Y}\widetilde{Y}'} + M_{\widetilde{Y}} \tan^2 \chi \,,
\tag{C3}
$$

as well as the mixing mass parameter between $U(1)_Y$ and $U(1)'$ gauginos

$$
M_{\widetilde{Y}\tilde{Z}'} = \frac{M_{\widetilde{Y}\widetilde{Y}'}}{\cos \chi} - M_{\widetilde{Y}} \tan \chi \,,
\tag{C4}
$$

all follow from the soft-breaking sector. Through the mixing of the gauge bosons, $M_{\tilde{Z}'}$ and $M_{\widetilde{Y}\tilde{Z}'}$ exhibit an explicit dependence on the masses of the $U(1)_Y$ and $U(1)'$ gauginos, and their mass mixing. $M_{\widetilde{Y}\widetilde{Y}'}$ is the soft-breaking mass that mixes the $U(1)_Y$ and $U(1)'$ gauginos. In the numerical analysis, we set the mixing mass parameter $M_{\widetilde{Y}\tilde{Z}'} = 0$ since we neglect the kinetic mixing ($\tan \chi \to 0$) thus $M_{\widetilde{Y}\widetilde{Y}'} \to 0$. For convenience we also define $R_{Y'} \equiv M_{\widetilde{Y}'}/M_{\widetilde{Y}}$.

The remaining entries in (C2) are generated by the soft-breaking masses in the Higgs sector via the $SU(3)_c \otimes SU(2)_L \otimes U(1)_Y \otimes U(1)'$ breaking. Their explicit expressions are given by

$$
\begin{aligned}
M_{\widetilde{Y}\tilde{H}_d} &= M_Z \sin \theta_W \cos \beta \,, \quad M_{\widetilde{Y}\tilde{H}_u} = M_Z \sin \theta_W \sin \beta \,, \\
M_{\widetilde{W}\tilde{H}_d} &= M_Z \cos \theta_W \cos \beta \,, \quad M_{\widetilde{W}\tilde{H}_u} = M_Z \cos \theta_W \sin \beta \,, \\
\mu_{H_d} &= h_s \frac{v_d}{\sqrt{2}} \,, \quad \mu_{H_u} = h_s \frac{v_u}{\sqrt{2}} \,, \quad \mu'_{H_d} = g_{Y'} Q'_{H_d} v_d, \\
\mu'_{H_u} &= g_{Y'} Q'_{H_u} v_u \,, \quad \mu'_S = g_{Y'} Q'_S v_s \,, \quad \mu'_{S_i} = g_{Y'} Q'_{S_i} v_{s_i} \,,
\end{aligned}
\tag{C5}
$$

where $g_{Y'}$ is the coupling constant of $U(1)'$. For numerical analysis we choose the standard GUT value for it $g_{Y'} = \sqrt{\frac{5}{3}} g \tan \theta_W$.

Appendix D: The Compositions of the Neutralinos

In this Appendix we give the Bino, Wino, Higgsino and Singlino compositions of the physical neutralinos $\widetilde{\chi}_i^0, i = 1, 2, ..., 9$ for the three scenarios LM1$'$, LM2$'$ and LM6$'$. They are listed in Table VI.

$LM1'$	$\tilde{\chi}^0_1$	$\tilde{\chi}^0_2$	$\tilde{\chi}^0_3$	$\tilde{\chi}^0_4$	$\tilde{\chi}^0_5$	$\tilde{\chi}^0_6$	$\tilde{\chi}^0_7$	$\tilde{\chi}^0_8$	$\tilde{\chi}^0_9$
$\tilde{B}$	-0.988	0.046	0.077	0.043	-0.056	0.095	-0.002	0.0	0.0
$\tilde{W}^3$	0.037	-0.058	0.955	-0.122	0.086	-0.245	0.006	0.0	0.0
$\tilde{H}^0_d$	-0.126	0.051	-0.245	-0.321	0.692	-0.581	0.014	0.0	0.003
$\tilde{H}^0_u$	0.031	-0.205	0.115	0.226	0.698	0.633	-0.033	0.002	-0.040
$\tilde{S}$	0.057	0.910	0.086	0.362	0.140	0.0	0.048	-0.004	0.087
$\tilde{Z}'$	-0.010	-0.180	-0.010	0.212	0.022	-0.092	0.065	0.013	0.953
$\tilde{S}_1$	-0.012	-0.148	-0.013	0.492	0.012	-0.276	-0.576	0.555	-0.133
$\tilde{S}_2$	-0.006	-0.089	-0.006	0.155	0.008	-0.060	0.778	0.586	-0.120
$\tilde{S}_3$	0.018	0.241	0.020	-0.621	-0.023	0.320	-0.232	0.589	0.223
$LM2'$									
$\tilde{B}$	0.048	-0.994	0.032	-0.009	-0.044	0.076	-0.005	0.0	0.0
$\tilde{W}^3$	-0.054	0.0101	0.974	0.029	0.067	-0.204	0.014	0.0	0.0
$\tilde{H}^0_d$	0.032	-0.088	-0.191	0.135	0.699	-0.666	0.043	0.0	0.001
$\tilde{H}^0_u$	-0.224	0.013	0.083	-0.062	0.692	0.673	-0.057	0.002	-0.033
$\tilde{S}$	0.942	0.054	0.075	-0.238	0.152	0.130	0.028	-0.003	0.069
$\tilde{Z}'$	-0.119	-0.006	-0.007	-0.190	0.015	-0.019	0.047	0.011	0.972
$\tilde{S}_1$	-0.091	-0.007	-0.010	-0.550	0.006	-0.143	-0.585	0.561	-0.100
$\tilde{S}_2$	-0.069	-0.005	-0.006	-0.212	0.005	0.013	0.778	0.578	-0.094
$\tilde{S}_3$	0.165	0.012	0.016	0.732	-0.013	0.123	-0.206	0.591	0.169
$LM6'$									
$\tilde{B}$	-0.036	-0.995	-0.034	-0.003	0.035	-0.072	0.006	0.0	0.0
$\tilde{W}^3$	0.041	0.015	-0.978	0.014	-0.054	0.194	-0.017	0.0	0.0
$\tilde{H}^0_d$	-0.015	-0.080	0.174	0.093	-0.700	0.677	-0.060	0.0	-0.002
$\tilde{H}^0_u$	0.196	0.021	-0.089	-0.015	-0.695	-0.680	0.073	0.001	0.031
$\tilde{S}$	-0.936	0.040	-0.057	-0.278	-0.143	-0.114	-0.028	-0.004	-0.073
$\tilde{Z}'$	0.138	-0.005	-0.006	-0.202	-0.012	0.007	-0.046	0.012	-0.967
$\tilde{S}_1$	0.116	-0.007	0.010	-0.541	-0.006	0.120	0.593	0.560	0.109
$\tilde{S}_2$	0.082	-0.004	0.005	-0.215	-0.004	-0.044	-0.772	0.581	0.101
$\tilde{S}_3$	-0.203	0.011	-0.015	0.729	0.012	-0.070	0.197	0.589	-0.185

TABLE VI. *The Bino, Wino, Higgsino and Singlino composition of the neutralinos $\tilde{\chi}^0_i, i = 1, 2, ..., 9$ for the scenarios* $LM1', LM2'$ *and* $LM6'$.

[1] J. E. Kim and H. P. Nilles, Phys. Lett. B **138**, 150 (1984); D. Suematsu and Y. Yamag-ishi, Int. J. Mod. Phys. A **10**, 4521 (1995) [arXiv:hep-ph/9411239]; M. Cvetic and P. Langacker, Mod. Phys. Lett. A **11**, 1247 (1996) [arXiv:hep-ph/9602424]; V. Jain and R. Shrock, arXiv:hep-ph/9507238; D. A. Demir, Phys. Rev. D **59**, 015002 (1999) [arXiv:hep-ph/9809358]; H. S. Lee, K. T. Matchev and T. T. Wang, Phys. Rev. D **77**, 015016 (2008) [arXiv:0709.0763 [hep-ph]].

[2] M. Cvetic and P. Langacker, Phys. Rev. D **54**, 3570 (1996) [arXiv:hep-ph/9511378]; M. Cvetic and P. Langacker, Mod. Phys. Lett. A **11**, 1247 (1996) [arXiv:hep-ph/9602424].

[3] J. L. Hewett and T. G. Rizzo, Phys. Rept. **183**, 193 (1989).

[4] C. T. Hill and E. H. Simmons, Phys. Rept. **381**, 235 (2003) [arXiv:hep-ph/0203079].

[5] P. Minkowski, Phys. Lett. B **67**, 421 (1977); R. N. Mohapatra and G. Senjanovic, Phys. Rev. Lett. **44**, 912 (1980).

[6] A. Bartl *et al.*, Phys. Lett. B **460**, 157 (1999) [arXiv:hep-ph/9904417]. A. Bartl, K. Hidaka, T. Kernreiter and W. Porod, Phys. Lett. B **538**, 137 (2002) [arXiv:hep-ph/0204071]; A. Bartl, K. Hidaka, T. Kernreiter and W. Porod, Phys. Rev. D **66**, 115009 (2002) [arXiv:hep-ph/0207186].

[7] J. Erler, P. Langacker and T. j. Li, Phys. Rev. D **66**, 015002 (2002) [arXiv:hep-ph/0205001].

[8] D. A. Demir, L. L. Everett, M. Frank, L. Selbuz and I. Turan, Phys. Rev. **D81**, 035019 (2010) [arXiv:0906.3540 [hep-ph]].

[9] G. L. Bayatian *et al.* [CMS Collaboration], J. Phys. G **34**, 995 (2007).

[10] M. Battaglia, A. De Roeck, J. R. Ellis, F. Gianotti, K. A. Olive and L. Pape, Eur. Phys. J. C **33**, 273 (2004) [arXiv:hep-ph/0306219].

[11] M. Battaglia, A. De Roeck, J. R. Ellis *et al.*, Eur. Phys. J. **C22**, 535-561 (2001) [hep-ph/0106204].

[12] D. N. Spergel *et al.* [WMAP Collaboration], Astrophys. J. Suppl. **170**, 377 (2007) [arXiv:astro-ph/0603449].

[13] D. A. Demir and Y. Farzan, JHEP **0603**, 010 (2006) [arXiv:hep-ph/0601096].

[14] D. A. Demir, L. L. Everett and P. Langacker, Phys. Rev. Lett. **100**, 091804 (2008) [arXiv:0712.1341 [hep-ph]].

[15] A. Ali, D. A. Demir, M. Frank and I. Turan, Phys. Rev. **D79**, 095001 (2009) [arXiv:0902.3826 [hep-ph]].

[16] B. C. Allanach, Comput. Phys. Commun. **143**, 305-331 (2002) [hep-ph/0104145].

[17] P. Bechtle, O. Brein, S. Heinemeyer *et al.*, Comput. Phys. Commun. **181**, 138-167 (2010) [arXiv:0811.4169 [hep-ph]].

[18] See the URL: http://theory.sinp.msu.ru/∼pukhov/calchep.html; A. Pukhov, arXiv:hep-ph/0412191.

[19] A. Semenov, arXiv:0805.0555 [hep-ph]; A. Semenov, Comput. Phys. Commun. **115**, 124 (1998).

[20] M. R. Whalley, D. Bourilkov, R. C. Group, arXiv: hep-ph/0508110.

[21] G. Belanger, F. Boudjema, A. Pukhov *et al.*, Comput. Phys. Commun. **180**, 747-767 (2009) [arXiv:0803.2360 [hep-ph]]; G. Belanger, F. Boudjema, P. Brun *et al.*, [arXiv:1004.1092 [hep-ph]].

[22] E. Komatsu *et al.* [WMAP Collaboration], arXiv:1001.4538 [astro-ph.CO].

[23] P. Konar, K. Kong, K. T. Matchev, JHEP **0903**, 085 (2009). [arXiv:0812.1042 [hep-ph]].

[24] T. Sjostrand, S. Mrenna and P. Skands, JHEP **0605** (2006) 026 [arXiv:hep-ph/0603175].

[25] M. Cvetic, D. A. Demir, J. R. Espinosa, L. L. Everett and P. Langacker, Phys. Rev. D **56**, 2861 (1997) [Erratum-ibid. D **58**, 119905 (1998)] [arXiv:hep-ph/9703317]; P. Langacker and J. Wang, Phys. Rev. D **58**, 115010 (1998) [arXiv:hep-ph/9804428].

[26] P. Langacker, arXiv:0801.1345 [hep-ph].

[27] For LEP bounds see: [LEP Collaboration], arXiv:hep-ex/0312023; For most recent bounds from Tevatron see: K. Hatakeyama [CDF Collaboration], arXiv:0810.3681 [hep-ex].

[28] U. Amaldi *et al.*, Phys. Rev. D **36** (1987) 1385; P. Langacker, M. x. Luo and A. K. Mann, Rev. Mod. Phys. **64**, 87 (1992); J. Erler and P. Langacker, Phys. Rev. Lett. **84**, 212 (2000) [arXiv:hep-ph/9910315]; Phys. Lett. B **456** (1999) 68; [arXiv:hep-ph/9903476].

[29] A. Fiandrino and P. Taxil, Phys. Rev. D **44**, 3490 (1991); P. Taxil, E. Tugcu and J. M. Virey, Eur. Phys. J. C **24**, 149 (2002) [arXiv:hep-ph/0111242].

[30] P. Langacker, R. W. Robinett and J. L. Rosner, Phys. Rev. D **30** (1984) 1470; F. del Aguila, M. Quiros and F. Zwirner, Nucl. Phys. B **284** (1987) 530; Nucl. Phys. B **287** (1987) 419; M. Cvetic and B. W. Lynn, Phys. Rev. D **35** (1987) 51; F. del Aguila, M. Cvetic and P. Langacker, Phys. Rev. D **48**, R969 (1993); Phys. Rev. D **52**, 37 (1995); F. Del Aguila and M. Cvetic, Phys. Rev. D **50**, 3158 (1994); A. Leike, Phys. Lett. B **402**, 374 (1997); Phys. Rept. **317**

(1999) 143; T. Appelquist, B. A. Dobrescu and A. R. Hopper, Phys. Rev. D **68**, 035012 (2003)
M. Dittmar, A. S. Nicollerat and A. Djouadi, Phys. Lett. B **583** (2004) 111; A. Freitas, Phys.
Rev. D **70** (2004) 015008; M. Carena, A. Daleo, B. A. Dobrescu and T. M. P. Tait, Phys. Rev.
D **70**, 093009 (2004); F. Petriello and S. Quackenbush, arXiv:0801.4389 [hep-ph].

[31] J. Kang and P. Langacker, Phys. Rev. D **71**, 035014 (2005).